IR TO VISIBLE UPCONVERSION

R. R. Zucca, et al

Rockwell International Corporation

Prepared for:

Advanced Research Projects Agency

10 December 1973

This research was supported by the Advanced Research Projects Agency of the Department of Defense and was monitored by SAMSO/DYJT under Contract No. F04701-71-C-0364.

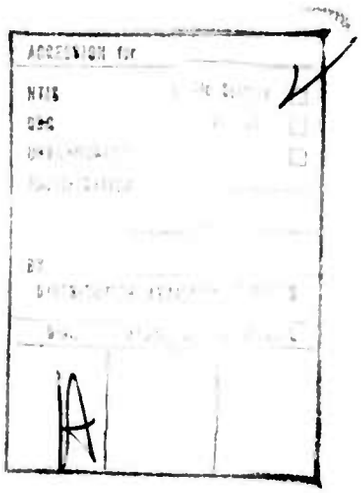

Unclassified

SECURITY CLASSIFICATION OF THIS PAGE (When Date Entered)

REPORT DOCUMENTATION PAGE

READ INSTRUCTIONS BEFORE COMPLETING FORM

1. REPORT NUMBER: TR73-377
2. GOVT ACCESSION NO.:
3. RECIPIENT'S CATALOG NUMBER: AD 771 592

4. TITLE (and Subtitle): IR TO VISIBLE UPCONVERSION

5. TYPE OF REPORT & PERIOD COVERED: Final; 1 April 1973 through 1 October 1973

6. PERFORMING ORG. REPORT NUMBER: SC517.26FR

7. AUTHOR(s):
R. R. Zucca
T. C. Lim

8. CONTRACT OR GRANT NUMBER(s): F04701-71-C-0364

9. PERFORMING ORGANIZATION NAME AND ADDRESS:
Science Center, Rockwell International
P. O. Box 1085, Thousand Oaks, CA 91360

10. PROGRAM ELEMENT, PROJECT, TASK AREA & WORK UNIT NUMBERS:
ARPA Order No.: 1629
Program Code No.: 3E50

11. CONTROLLING OFFICE NAME AND ADDRESS:
Advanced Research Projects Agency
1400 Wilson Boulevard
Arlington, VA 22209

12. REPORT DATE: December 10, 1973

13. NUMBER OF PAGES: 66

14. MONITORING AGENCY NAME & ADDRESS (if different from Controlling Office):
Department of the Air Force
HQ Space & Missile Systems Orgn. (AFSC)
P. O. Box 92960, Worldway Postal Center
Los Angeles, CA 90009

15. SECURITY CLASS. (of this report): Unclassified

15a. DECLASSIFICATION/DOWNGRADING SCHEDULE:

16. DISTRIBUTION STATEMENT (of this Report):

Approved for public release; distribution unlimited

17. DISTRIBUTION STATEMENT (of the abstract entered in Block 20, if different from Report):

18. SUPPLEMENTARY NOTES:

19. KEY WORDS (Continue on reverse side if necessary and identify by block number):

Upconversion
IR-Visible Upconversion
Chemical Vapor Deposition
Doping
ZnS
Luminescence
III-V Heterojunction

20. ABSTRACT (Continue on reverse side if necessary and identify by block number):

This report contains two approaches to the problem of infrared-to-visible conversion for thermal imaging--IR-induced luminescence in a phosphor (ZnS) and a semiconductor heterostructure. Upconversion in ZnS doped with Cu and Cl (or Al) takes place by luminescent decay of electrons trapped at the Cl sites after excitation from Cu sites by UV radiation. Doped epitaxial films of ZnS were grown by chemical vapor deposition (CVD) on undoped ZnS substrates. The first measurements of spectral dependence and temperature dependence of the upconversion emission are presented and discussed. The internal quantum efficiency is

DD FORM 1 JAN 73 1473 EDITION OF 1 NOV 65 IS OBSOLETE

Unclassified

SECURITY CLASSIFICATION OF THIS PAGE (When Date Entered)

20. low, of the order of 10^{-4}. However, the UV-induced IR absorption is very high (of the order of 800 cm^{-1}). Measurements of transient effects indicate that such high absorption is connected with a non-visible luminescent process. This implies that more investigation of this effect could lead to and increase of the internal quantum efficiency. The proposed heterostructure approach is very similar to a heterojunction photocathode, with electrons being excited in a small-gap material and decaying in a large-gap material. Preliminary studies were done on CVD growth of high-quality epilayers of n-type $InAs_{1-x}P_x$ on p-type InAs substrates with and without grading of the junction. Measurements of the photoresponse indicate that photogenerated electrons are transported more effectively in the graded material. The capability of grading and the ease of doping show that CVD is a powerful tool to realize complicated layer structures.

TR73-377

SC517.26FR

IR TO VISIBLE UPCONVERSION

Final Report (Part II) for the Period
1 April 1973 through 1 October 1973

December 10, 1973

Contract No. F04701-71-C-0364

ARPA Order No.: 1629
Program Code No.: 3E50
Effective Date of Contract: 73 April 01
Contract Expiration Date: 73 October 01
Amount of Contract: $90,000
Principal Investigators:
R. R. Zucca (805) 498-4545, X-420
T. C. Lim (805) 498-4545, X-418
Project Scientist:
A. S. Joseph (805) 498-4545, X-116

Approved for public release; distribution unlimited.

Approved by

A. S. Joseph
Director
Solid State Electronics

Science Center
Rockwell International

TABLE OF CONTENTS

FIGURE CAPTIONS

Page

FOREWORD

This report was prepared by the Rockwell International Corporation under contract F04701-71-C-0364, Advanced Development Program 3E50. This report covers the period 1 April 1973 through 1 October 1973 and is the Final Report on this contract. The work described herein was carried out by the Science Center, Rockwell International, Thousand Oaks, California.

The project engineer at the Science Center, Rockwell International, for this effort was Dr. R. R. Zucca, and the associate project engineer was Dr. T. C. Lim.

The program manager was Dr. A. L. Joseph.

The principal technical support for this work was carried out at the Science Center by E. S. Cory, G. P. Espinosa, and D. H. Hengstenberg.

ABSTRACT

This report contains two approaches to the problem of infrared-to-visible conversion for thermal imaging--IR-induced luminescence in a phosphor (ZnS) and a semiconductor heterostructure. Upconversion in ZnS doped with Cu and Cl (or Al) takes place by luminescent decay of electrons trapped at the Cl sites after excitation from Cu sites by UV radiation. Doped epitaxial films of ZnS were grown by chemical vapor deposition (CVD) on undoped ZnS substrates. The first measurements of spectral dependence and temperature dependence of the upconversion emission are presented and discussed. The internal quantum efficiency is low, of the order of 10^{-4}. However, the UV-induced IR absorption is very high (of the order of 800 cm^{-1}). Measurements of transient effects indicate that such high absorption is connected with a non-visible luminescent process. This implies that more investigation of this effect could lead to an increase of the internal quantum efficiency. The proposed heterostructure approach is very similar to a heterojunction photocathode, with electrons being excited in a small-gap material and decaying in a large-gap material. Preliminary studies were done on CVD growth of high-quality epilayers of n-type $InAs_{1-x}P_x$ on p-type InAs substrates with and without grading of the junction. Measurements of the photoresponse indicate that photogenerated electrons are transported more effectively in the graded material. The capability of grading and the ease of doping show that CVD is a powerful tool to realize complicated layer structures.

UPCONVERSION OF INFRARED TO VISIBLE
FINAL REPORT

1.0 INTRODUCTION

Since there is an atmospheric window for IR transmission at 10μ and because room temperature thermal radiation peaks in this region, there are military needs for passive imagery systems of high efficiency in this spectral range.

Various concepts have been studied for implementing the above requirement. These approaches can be grouped in two categories: the detector array, where the IR radiation is converted into an electrical signal and then electronically processed to a visible display, and the upconverter that converts IR photons directly into visible photons inside some upconversion material.

Good detectors are available, but since arrays require large numbers of sensors of uniform response, serious processing problems arise. Furthermore, the implementation of arrays requires, in principle, complicated systems. Systems employing upconverters are conceptually much simpler, since the conversion takes place in the material without need of external circuitry. However, fundamental questions on material properties and device principles have still to be answered before a judgment can be made on the ultimate qualities that can be expected from upconverters.

In this report two approaches to the upconversion problem are explored. One is the phosphor upconverter, which utilizes the IR-stimulated luminescence of ZnS. The other is a heterojunction system where electrons

excited by the IR radiation in a small-gap semiconductor are transported into a large-gap material, where they decay emitting visible light. Although the two approaches have the utilization of chemical vapor deposition (CVD) facilities for crystal film growth in common, they involve totally different concepts. Therefore, this report is divided into two separate parts each with the structure of a separate report. Sec. 2 contains the discussion of the phosphor (ZnS) upconverter, and Sec. 3 the discussion of the hetero-structure approach.

2.0 PHOSPHOR UPCONVERTER REPORT

2.1 INTRODUCTION

It is well known that if a doped phosphor is stimulated with ultraviolet light, visible luminescence associated with impurities and native defect states is observed. In addition, if the sample is illuminated with IR after ultraviolet excitation the visible radiation is enhanced. This phenomenon, called upconversion, has the potential of being used for thermal imaging in the 10μ region of the spectrum.[1-3] To date, because of the lack of control on material preparation, it has been difficult to perform systematic studies aimed at understanding the relationship between the stimulation and luminescence mechanism.

Briefly describing the processes involved allows us to obtain some insight into the problem. Consider the specific case of ZnS doped with the activator Cu and a co-activator such as Al in equal concentrations. Figure 1 helps in understanding the general concepts. The figure represents the energy diagram in real space and illustrates, schematically, the potential wells for the donor-acceptor states. Since Al has one excess electron and Cu is one electron deficient with respect to Zn, the acceptor states will be populated by the excess electrons from the donor dopants. When the phosphor is illuminated with UV radiation, the electrons in the valence band and on the Cu sites will be excited to unoccupied donor levels. The donor-acceptor states with small separation distance r (see Fig. 1) will recombine at low temperatures, primarily by a tunneling mechanism with a probability proportional to the overlap of the wave functions in the respective wells. This leads to luminescence (the so-called green Cu luminescence[4]) in the absence of IR

stimulation. The donor-acceptor states with large r have a smaller tunneling probability and hence have a longer lifteime for recombination. If now the sample is exposed to IR radiation containing energies corresponding to the depth of the potential well of the donor states, trapped electrons can recombine with acceptor states via the conduction band. This can be accomplished by recapture in an acceptor-donor combination with small r or direct recombination from the conduction band. The visible recombination emission, often called IR-stimulated luminescence, constitutes the upconverted light emission.

The achievement is remarkable: 10μ infrared photons are converted into visible (green) photons by a process that takes place internally in a crystal requiring only outside UV excitation. However, three difficulties prevent such a simple concept from immediate application.

1. The upconversion process can be observed only at low temperature. This restriction is typical of 10μ detection systems of high sensitivity. Low temperature is necessary in order to reduce thermal noise generation.
2. In spite of the simplicity of the process, the system implementation is not ideal. The phosphor must be periodically excited with UV light. After the UV is turned off the ordinary luminescence contributes to noise superimposed on the upconversion emission. Such a drawback must be looked upon in the context of other available thermal imagery systems to realize that such complications are small in comparison. Furthermore,

high efficiency would make such difficulties tolerable.

3. Efficiencies, defined as the ratios of the number of emitted visible photons to the number of incident IR photons, are low. Efficiencies better than 10^{-3} have not been reported.[3] However, no effort has been made to optimize the efficiency, and some of the physical processes that determine the efficiency have not been clarified.

It is clear that any judgment on the ultimate quality of a phosphor upconverter depends on the understanding of the physical processes that limit the efficiency.

The donor-acceptor model discussed above gives some insight into the critical parameters contributing to the efficiency.

1. One should not expect to increase the IR-to-visible conversion by continuously increasing the concentration of dopants. This follows since the metastable states, which are stimulated by IR, require donor-acceptor states of large r. Increasing the concentration should eventually lead to a decrease in the up-converted emission. Hence, there exists a concentration for which the efficiency is maximized.
2. A major degradation of the efficiency appears to be caused by the low IR absorption by the luminescence radiation centers.[3] Here progress can be made by a better understanding of the impurities energy level scheme. The energy levels of Cu in ZnS have been extensively studied,[4] but very little is known of

the energy level scheme of the co-activators.[5] It is crucial to have a better understanding of the decay mechanisms that compete with visible photon emission once an IR photon is absorbed. Also, the role of native defects, abundant in II-VI compounds, needs clarification.

Previous to this, all the studies of ZnS luminescence have been done on doped powders or on bulk single crystals which were grown from powders. However. recently we were able to grow epitaxial films of ZnS on GaAs substrates by chemical vapor deposition (CVD). The films had either zincblende or wurtzite crystal st.ucture depending on growth condition. Since CVD films are grown at lowe· temperatures than bulk-grown crystals, they have lower impurity concentration and fewer defects. Since defects and impurities play a key role in upconversion, it is very beneficial to perform experiments on CVD-grown films.

This work has two phases. First, grow thick films of ZnS doped with Cu as the activator and Al or Cl as a co-activator, Al substituting for Zn or Cl substitu·ing for S in the crystal. Second, perform studies of the upconversion effect in order to evaluate the efficiency and analyze the physical processes that determine this efficiency.

In light of the extremely short time available (six months), it was impossible to follow the above program exhaustively. The time available would have been insufficient to cover even one of the two phases in full. Therefore, a thorough review of phosphor upconverters was not attempted. However, the two phases described above were completed. The potential of CVD-grown ZnS

for upconverter applications was explored, and some contributions to the understanding of the upconversion effect were made. It is hoped that this work will serve as a guideline for future work on this problem.

2.2 EXPERIMENTAL APPROACH

The work involves the growth of doped ZnS films by chemical vapor deposition (CVD) and the study of the upconversion effect in such films. Two experimental facilities were used for this activity. One is a CVD reactor, the other an optical facility to perform combined photoluminescence and IR transmissivity measurements on samples at variable low temperatures. In the next two sections the crystal growth techniques and the optical evaluation system are described.

2.2.1 Crystal Growth

A unique chemical vapor deposition (CVD) system was utilized to produce high quality ZnS epitaxial films. A photograph of the system is shown in Fig. 2, and a schematic of the reactor is shown in Fig. 3. There are six zones where the temperature profile may be adjusted to obtain optimum growth conditions.

As a result of studies on the growth of high-quality ZnS films, the following optimum conditions for the gases were determined. The flow rate for H_2S is about 3 cc/min, for the carrier gas (H_2) which mixes with H_2S about 900 cc/min, and for Zn about 300 cc/min. It was found that the transport rate of zinc is important towards obtaining single crystalline films. The optimum transport rate for zinc was found to be about 2×10^{-4} moles/min. The phase transition of ZnS (from wurtzite to sphalerite) occurs

at about 1024°C. Therefore, in order to obtain a sphalerite-phase film, the growth temperature has to be below 1000°C. It was found that the optimum temperature for growing such a film on GaAs is about 900°C. The optimum growth rate at that temperature is about 15μ/hr. Further increase or decrease in temperature results in a slower growth rate. The quality of the films far exceeds that of any film described in the scientific literature. In particular, the surface quality is far smoother than that previously reported.[8] The principal reason for this success is an ability to determine the optimum zone for deposition. The deposition length ℓ is related to the gas flow velocity and the diffusion constant by

$$\ell = \frac{9}{16} \frac{V_{av} Y^2}{D_{AB}}$$

where V_{av} is the average flow velocity, Y the diameter of the reactor, and D_{AB} the diffusion constant of molecules Zn and H_2S. This length is vital for obtaining good single crystalline film because deviation from this distance results in a non-stoichiometric film.

The operational mode for doping crystals, so that they have the desired optical properties, consists of strict feedback between crystal growth and optical evaluation. Films were evaluated immediately after being grown, this evaluation was done mostly by photoluminescence measurements at liquid He temperature. In order to determine that a given luminescence peak was due to certain dopants, the luminescence spectra of samples with increased and decreased concentrations of that dopant were compared. This procedure was easily applied to CVD-grown materials, since the CVD growth process is fast.

By growing thin films for quick evaluation purposes, one full feedback loop of growth and optical evaluation required only a day.

2.2.2 Optical Measurements

Figure 4 is a photograph of the facility for optical measurements, and Fig. 5 a block diagram of the system. In the upper right portion of the block diagram is seen the photoluminescence portion of the facility. Radiation from a UV source chopped at a frequency ω_{UV} = 550 Hz is focused on the sample. The radiation emitted from the sample is analyzed by a system consisting of a 1-meter Czerny-Turner spectrometer, an EMI 9558Q photomultiplier, a lock-in detector controlled by ω_{UV}, and a dual pen recorder. The system has been calibrated for absolute power against the emission of a standard lamp. After a luminescence spectrum is digitized on a graphic digitizer, a computer program corrects for the spectral response of the system and plots the corrected spectrum. The UV source is a 100 watt high-pressure Hg lamp. Most of the experiments were performed using the 3650Å line of the Hg spectrum which was found to be the most efficient for the excitation of the ZnS luminescence.

The remaining portion of the block diagram shows a two-beam system for measurements of optical transmissivity in the infrared. Monochromatic light form the 0.3m monochromator is divided by a beam splitter into a reference beam chopped at frequency ω_R = 200 Hz, and a sample beam chopped at a frequency ω_S = 150 Hz. Both beams are optically equivalent, except that one beam passes through the sample. The detector is a PbSnTe photodiode made in this laboratory. The electronic signals of the two beams are separated by two lock-in amplifiers. The reference signal controls the gain of the system with an

automatic gain control (AGC) unit. This compensates for the spectral changes of signal intensity. The transmissivity spectrum is automatically plotted. Changing the position of mirror M allows for reflectivity measurements. The IR light source is normally a Nernst glower, but a 10.6μ CO_2 laser may be substituted when high power is required.

The sample is held in a Heli-Tran dewar manufactured by Air Products and Chemicals. This dewar consists of a variable temperature cold finger with a cold radiation shield. Being of the cold-finger type, there is some uncertainty as to sample temperature because of temperature gradients between the sample and the sample holder where the temperature is measured. But even errors of 2 or 3°K are unimportant for this purpose. The advantage of the cold-finger dewar is that a simple design of the tail is allowed. It does not require the double windows of immersion dewars. The tail used has a hexagonal shape with quartz windows for the UV and KBr windows for the IR.

Having a transmissivity and a photoluminescence system that can operate simultaneously on the same sample allows the performance of a variety of experiments. In addition to photoluminescence and transmissivity, the following experiments, when both the IR and UV radiation are simultaneously applied to the sample, can be performed:

1. <u>UV-Induced IR Absorption</u>: This can be measured by comparing the transmissivity spectra with the UV light on to the one with the UV light off. However, this can also be observed directly if the reference signal for the sample lock-in amplifier, normally taken from the chopper at ω_S, is instead taken from the UV chopper at ω_{UV}. When used this way the detected

sample signal has an amplitude proportional to the change of transmissivity induced by the UV radiation. However, care must be exercised. If the UV-induced IR absorption has a time constant comparable to the switching time of the UV chopper, the signal amplitude becomes dependent on the chopping frequency ω_{UV}.

2. IR-Induced Luminescence (Upconversion): This is measured by connecting a second lock-in amplifier in parallel with the photoluminescence lock-in amplifier at ω_{UV}. This second lock-in amplifier (not shown in Fig. 5) takes its reference signal from the IR chopper at ω_S, and detects only luminescent emission triggered by the IR radiation at frequency ω_S, while the ordinary luminescence is filtered out as noise. At the same time, the lock-in amplifier at ω_{UV} records the ordinary luminescence. It is also possible to remove the UV chopper and observe only the upconversion signal. In this mode the intensity of the upconversion signal is doubled since the UV excitation is on full time instead of half time.

In practice, any two of the four types of measurements described in this section photoluminescence, IR transmission, UV-induced IR absorption and upconversion can be made simultaneously. This flexibility was convenient for the type of measurements reported in Section 3.2, for example, comparison of photoluminescence and upconversion spectra, IR power dependence of upconversion, temperature dependence of IR absorption and upconversion, etc. Such experiments require the measurement of two effects at the same time.

2.3 RESULTS AND DISCUSSION, MATERIAL TECHNOLOGY

2.3.1 Undoped Films

Before this project, thin epitaxial films of ZnS on GaAs substrates had been grown. In Fig. 6 an X-ray diffractometer measurement on a ZnS film grown on the (100) plane of a GaAs substrate is shown. The film has zinc-blende structure and is of good quality. However, since there is a 4.5% lattice mismatch between GaAs and ZnS, a regular array of parallel cracks with spacing of the order of 200μ appear on the film. Such cracks are of no concern for upconversion, since the distance between cracks is orders of magnitude larger than the mean free path of the photoexcited electrons.

Before doping was considered, it was necessary to improve the growth techniques to achieve thick films. Figure 7a shows the side view of an unpolished film of cubic ZnS on the (001) plane of GaAs. The film thickness is about 80μ. Since the film was grown at a fast rate (typically 15μ/hr), the finished surface was rough. Having developed a technique of polishing (Fig. 7b), it was found more efficient to operate at a fast rate of growth resulting in a rough surface, rather than a slow growth rate which leads to a higher degree of surface smoothness.

It was found that strong doping effects take place between the ZnS film and the GaAs substrate. Zn from ZnS diffuses into GaAs. This was suggested by measurements of the IR transmissivity of the film and substrate between 0.8 and 17μ. The transmissivity spectrum shows a broad absorption increasing toward the long wavelength with the typical shape of free carrier absorption. The ZnS films have a high resistivity after growth. Since the GaAs substrate has a high resistivity and is IR-transparent before the film

is grown, it was concluded that Zn diffuses into GaAs. This was confirmed by the appearance of the characteristic luminescence peak of Zn-doped GaAs at 8340Å when luminescence of the GaAs substrate is observed through the transparent ZnS film at 77°K.

Doping of the ZnS film by Ga from the substrate has also been observed. Photoluminescence measurements on the films at 4.2°K show a strong peak at 4650Å, which is characteristic of the self-activated luminescence of ZnS.[4] This same peak was observed in polycrystalline films of ZnS grown on quartz when a GaAs crystal was placed near the quartz substrate in the CVD reactor. Auger spectroscopy measurements also confirmed the existence of Ga in the ZnS film.

In principle, the diffusion of small amounts of Ga into the ZnS film would be beneficial since Ga is one of the impurities that could be used as a co-activator in upconversion. However, such large amounts of Ga diffuse into the film that the 4650Å luminescence totally dominates the luminescence spectrum of Cu-doped films.

Consequently, it was decided to grow films for upconvers on on bulk. grown, undoped ZnS substrates. The substrates were supplied by Eagle-Picher. The X-ray measurements indicate that the substrates are 6H-II polytypes of the wurtzite structure.

The ZnS films were grown on ZnS substrates under similar conditions to the ones grown on GaAs. X-ray measurements by Laue diffraction and by the precession method indicate that the crystal structure of the film is indistinguishable from that of the substrate.

Lack of discontinuity between film and substrate makes it difficult to measure the thickness of the films after grown. However, since the films of interest were Cu-doped, measurements were made by a staining technique.

2.3.2 Al-Doped Films

Al-doped ZnS films were grown on ZnS substrates. Al was transported by HCl gas. Presence of aluminum in the film has been confirmed by observing the blue self-activated luminescence.

It was somewhat difficult to distinguish between the blue luminescence of Cl and that of Al because of the scatter between the peak position reported by different experimenters.[4] Therefore, comparisons of measurements on Al-doped films with measurements on films grown under similar rates of HCl gas, but without transporting any Al were made. It was determined that the self-activated Cl luminescence peaks at 4650Å and that of Al at 4770Å, at room temperature. By this simple procedure, verification of efficient Al transport was made. It is suspected that some chlorine inclusion is still present in the films, even when the chlorine luminescence no longer appears.

In Fig. 8 the photoluminescence spectrum at 4.2°K of an Al-doped ZnS film grown on a ZnS substrate is shown. The peak shifts very little with temperature. The shift is toward higher energy when the temperature is decreased, as is common in semiconductor spectra. This result does not agree with the direction of the shift reported by others.[8]

2.3.3 Cu-Doped Films

Since copper metal is a low-vapor-pressure material, transporting it requires a volatile compound. Copper chloride was chosen. Helium is used as a carrier gas. Since the carrier gas for Zn is hydrogen, the helium flow rate has to be about 10 cc/min in order to prevent the CuCl from reducing inside the nozzle. Typical growth rates are ~ 10μ/hr. Approximately 40 atomic parts per million of Cu, as verified by chemical analysis, was transported. Photoluminescence measurements show a very strong peak at 5230Å 2.37 eV) at liquid He temperature. This green luminescence requires both an activator, Cu, and a co-activator. By exclusion of all other dopants, the co-activator must be Cl from the CuCl gas.

2.3.4 Doping for Upconversion

At this point, two co-activators were available to use with the activator Cu for upconversion--Cu or Al. The reason Al was preferred was that the only reported upconversion effects in single crystals were on Cu-Al-doped samples [3,5]

Using the experience gained in transporting Cu and Al individually, it was then possible to transport both dopants, simultaneously, in the same dopant tube by carrying them with HCl and He gases. Tne photoluminescence spectra show some green Cu luminescence, but there is a dominant blue luminescence. This dominant blue luminescence is attributed to excess Cl, which is present, because HCl was used to transport both the Cu and Al. The intensity of the blue luminescence was reduced by lowering the flow rate of HCl, but only at the expense of a drastic reduction of the Al content. It was concluded that with the present technique it is not possible to transport

Cu and Al without a significant amount of Cl. A better method may be to transport Al in a separate doping tube.

On the other hand, transporting Cl as a co-activator is quite easy. Cl is transported with the CuCl and by adding some HCl gas, the amount of Cl available for deposition on the film is increased, insuring that it equals or exceeds the amount of Cu. Although no upconversion has been reported from Cu-Cl-doped single crystals, there is no reason why Cl substituting S should not play the same donor role as Al substituting Zn. As discussed in the next section, this judgment is correct.

Figure 9 shows some photographs of a sample doped with Cu and Cl. The surface is extremely smooth--to the point that the sample scatters little light. This sample was used for transmissivity measurements without need of polishing. For this reason this sample was used for most of the upconversion measurements. The thickness of the film is 10μ. The Cu concentration was measured by mass spectroscopy on a film on a quartz blank that was near the sample in the CVD reactor. It was found to be 33 atomic parts per million. In Fig. 10 the photoluminescence spectrum of this film is shown at 4.2°K. The large peak, at 5230Å (2.37 eV) corresponds to the green luminescence. The smaller peak in the blue at 4520Å (2.74 eV) corresponds to the self-activated luminescence of Cl as determined by previous tests. This peak is an indication that the concentration of Cl exceeds that of Cu. When the amount of HCl is increased, the intensity of the blue luminescence also increases.

The luminescence of the Cu-doped samples is quite intense, so much

so that the interior of the dewar appears illuminated by green light. The green luminescence follows a decay law of the type $t^{-1.6}$, in agreement with previous reports.[7] This decay law, with a long persistent tail, can also be directly appreciated because the sample shows residual luminescence visible to the eye minutes after the UV excitation is turned off.

2.4 RESULTS AND DISCUSSION, UPCONVERSION STUDY

2.4.1 Upconversion Effect

The experimental arrangement has been described in Section 2.2. The upconversion effect has been detected with the Nernst glower as the IR source. However, in order to improve the S/N ratio, most measurements reported in this section were made with a CO_2 laser operating in a milliwatt range. The samples used were ZnS films doped with Cu and Cl as described in Section 2.3.4. The measurements were made at liquid He temperature, except when measuring the temperature dependence of the upconversion effect.

The upconversion effect is strong enough to be seen with the eye. The following procedure was used. The UV excitation was on for at least a few seconds, in order to populate the excited energy states. After the UV is turned off, only the long persistent portion of the luminescence is left as a weak background. The IR laser source is then turned alternately on and off. A sharp increase in the green luminescence is clearly seen on the sample where the IR beam is incident.

It seems natural to see upconversion in a single crystal sample in which Cl, instead of Al, is the co-activator since Cl acts as a donor, very much like Al. This has been confirmed by the similarity between the luminescence

spectra of Cu-Al and Cu-Cl doped crystals. However, this is the first time the upconversion effect has been observed in Cu-Cl doped single crystals. It is presumed that in previous experiments on bulk-grown single crystals,[5] the concentration of Cl was difficult to control.

Figure 11 shows the spectrum of the IR-stimulated luminescence (upconversion) and the normal photoluminescence of the sample of Fig. 9. This is the first time the spectral dependence of the upconverted signal has been measured. The similarity of the two curves is striking. This similarity proves that the decay process, stimulated by the IR radiation, is of the same nature as the ordinary luminescence; i.e., the IR photons act as "triggers" to release additional luminescence.

Upconversion effects in the blue have not been previously reported. The near identity of the two spectra of Fig. 11 includes the blue peak of the self-activated luminescence at 4520Å. Figure 12 shows the luminescence and upconversion spectra of a sample more rich in Cl. Here the blue luminescence is dominant. Nevertheless, the upconversion spectrum still reproduces the shape of the luminescence spectrum accurately.

A simple interpretation for the blue upconversion peak is that electrons trapped at Cl sites of slow spontaneous decay are excited into the conduction band by the IR photons. Once in the conduction band, the electrons are thermalized by scattering and they lose memory of their original impurity site. Finding themselves in the same condition as the electrons excited by UV radiation in the normal luminescence process, the upconversion electrons decay with a spectrum identical to that of the ordinary luminescence. This interpretation is totally independent of what the actual mechanism for blue self-activated luminescence is.

The blue upconversion observed may also be explained as an effect that takes place independent of the green upconversion effect. However, it would be hard to accept that two independent processes would have yields close enough that the upconversion and the luminescence spectra would look identical. Furthermore, tests made on samples with only the blue self-activated luminescence showed no upconversion effect.

After several days of exposure to the air, the samples show an aging effect. Aging reduces both the luminescence and the upconversion yields; the blue portion of the upconversion spectrum is the most affected. It is suspected that contaminants are producing surface absorption of the emitted visible photons. This problem requires more clarification.

Fundamental process, in the upconversion effect, is the IR absorption induced by the UV excitation. Figure 13 shows the spectral dependence of the UV-induced IR absorption on the sample of Fig. 9. The shape of this spectrum agrees in general with the transmission spectrum of Ref. 3. The absorption is very large. At 10.6μ the UV-induced absorption coefficient is 820 cm^{-1}. This is commented on further in the next sections.

2.4.2 Upconversion Efficiency

Since ambiguities often occur, a definition of terms is presented here. The external quantum efficiency η_E is defined as the ratio of the total number of emitted visible photons to the number of IR photons penetrating the sample. The internal quantum efficiency η_I is defined as the ratio of the total number of emitted visible photons to the number of IR photons absorbed by the sample.

At an IR power of 23 mW, the external quantum efficiency of the sample of Fig. 9 is $\eta_E = 4.3\times10^{-6}$, the internal quantum efficiency is $\eta_I = 1.2\times10^{-6}$. These values are at high IR power. For imaging application, the low power behavior must be investigated.

Figure 14 shows the total power emitted in the visible as a function of the IR power that penetrates the sample. Departure from a straight line indicates saturation effects, which imply a higher efficiency at low power.

The data of Fig. 14 can be fit to a straight line in a log-log plot, as in Ref. 3. This implies that $P_{UC} = KP_{IR}^n$, where P_{UC} is the emitted UV power, P_{IR} is the incident power and K and n are constants. However, the points of Fig. 14 would then be fit by a curve with $n < 1$, leading to the unrealistic conclusion that $P_{UC} \to \infty$ as $P_{IR} \to 0$. This implies that the efficiency goes to infinity.

It is preferable to develop a physical model which leads to an equation that may be extrapolated to low powers. In the simplest conceivable model, a set of IR-absorbing traps is populated at a constant rate T_{UV} by

2.4.2 Upconversion Efficiency

Since ambiguities often occur, a definition of terms is presented here. The external quantum efficiency η_E is defined as the ratio of the total number of emitted visible photons to the number of IR photons penetrating the sample. The internal quantum efficiency η_I is defined as the ratio of the total number of emitted visible photons to the number of IR photons absorbed by the sample.

At an IR power of 23 mW, the external quantum efficiency of the sample of Fig. 9 is $\eta_E = 4.3\times10^{-6}$, the internal quantum efficiency is $\eta_I = 1.2\times10^{-6}$. These values are at high IR power. For imaging application, the low power behavior must be investigated.

Figure 14 shows the total power emitted in the visible as a function of the IR power that penetrates the sample. Departure from a straight line indicates saturation effects, which imply a higher efficiency at low power.

The data of Fig. 14 can be fit to a straight line in a log-log plot, as in Ref. 3. This implies that $P_{UC} = KP_{IR}^n$, where P_{UC} is the emitted UV power, P_{IR} is the incident power and K and n are constants. However, the points of Fig. 14 would then be fit by a curve with $n < 1$, leading to the unrealistic conclusion that $P_{UC} \to \infty$ as $P_{IR} \to 0$. This implies that the efficiency goes to infinity.

It is preferable to develop a physical model which leads to an equation that may be extrapolated to low powers. In the simplest conceivable model, a set of IR-absorbing traps is populated at a constant rate T_{UV} by

the UV radiation; two competing processes, IR absorption and luminescence, deplete the traps at rates T_{IR} and T_L. If n is the occupation density of the traps and t is time, the conservation of particles leads to the rate equation

$$\frac{dn}{dt} = T_{UV} - T_L - T_{IR} \tag{1}$$

A reasonable assumption is that the transition rates T_L and T_{IR} are proportional to the density of available particles n, and that T_{IR} is proportional to the incident IR power P_{IR},

$$T_L = K_L n \tag{2}$$

$$T_{IR} = C_{IR} P_{IR} n \tag{3}$$

where K_L and C_{IR} are constants. For a steady-state condition, $dn/dt = 0$. From this, solving Eqs. (1), (2), and (3)

$$T_{IR} = \frac{T_{UV}}{1 + K_L/C_{IR}P_{IR}} = \frac{T_{UV}}{1 + 1/\beta P_{IR}} \tag{4}$$

where $\beta = C_{IR}/K_L$ is a constant. Assuming that the upconverted power, P_{UC} is proportional to the rate of IR absorption T_{IR}, the final expression becomes

$$P_{UC} = \frac{K}{1 + 1/\beta P_{IR}} \tag{5}$$

where K is a constant.

In Fig. 14, the solid line represents a least square fitting of the experimental points using Eq. (5). The fit is good with parameters $K = 4.03\mu W$ and $\beta = 0.046 mW^{-1}$.

At low power, the first term of a series expansion of Eq. (4) yields $P_{UC} \simeq K\beta P_{IR}$. From this the low power internal quantum efficiencies can be extrapolated, giving $\eta_I = 2.6\times10^{-5}$. A measurement of quantum efficiency with the Nernst glower as IR source, at an IR power level of only 25mW yields a still better value: $\eta_I = 10^{-4}$. This implies that the model needs some refinement to better describe the low power response.

With the electronic system operating at a bandwidth of 1 Hz, the minimum detectable IR power density is $\sim 10^{-7}$ Wcm^{-2}.

One conclusion from the above measurements is that the quantum efficiency for the CVD samples was low, the best figure we can report for η_I being 10^{-4}. From S/N ratios it is believed that some samples, on which quantum efficiency measurements were not made, have larger values, but even quantum efficiencies in the 10^{-3} range are too low. However, doping concentration studies to optimize the efficiency were not done due to time limitations. Since the efficiency must depend critically on doping concentrations, such studies are necessary.

The low values of internal quantum efficiency indicate that strong IR absorption processes, which lead to non-radiative decay, are taking place. This is confirmed in the next section. Extensive study to determine the nature of the competing processes is necessary.

2.4.3 Time and Temperature Dependence

When the UV excitation is turned off, the luminescence, the IR-stimulated luminescence (upconversion), and the UV-induced IR absorption show long persistent decays. The decay of the green luminescence has been studied by Era, et al.[7] The long persistent decay, indicated by triangles in Fig. 15a, follows approximately a t^{-n} dependence, n being a constant. This decay is typical of pair recombination.[9] A least square fit yields n = 1.36. This is of the same order as reported values.

In Fig. 15a the circles represent, on a log-log scale, the UV-induced absorption coefficient at the CO_2 laser wavelength (10.6μ) as a function of time after the UV is turned off. The points are well fitted by a straight line; i.e., a t^{-n} decay with n = 0.48. This decay is extremely slow. It requires 15 sec for α to decay to 0.1 of its initial value.

The decay of the IR absorption is much slower than that of the luminescence. This implies that most of the IR absorption centers generated by the UV excitations decay spontaneously by a means other than visible luminescence.

In Fig. 15b the circles represent, also on a log-log scale, the upconverted emission intensity as a function of time after the UV is turned off. An interesting feature is the change of slope after the first 4 seconds of decay. The curve is well fitted by a linear combination of two t^{-n} curves as shown by the solid line in Fig. 15b. A least square fit yields n = 1.63, close to the value for the luminescence (n = 1.36), for the second term n = 0.44, close to the value for the IR absorption (n = 0.48). This can be seen when comparing the two curves of Fig. 15a with that of Fig. 15b.

The correlation between the slopes of the three decays, is interpreted as follows. Electrons that were released by the IR, when the UV was on, are initially available. Such electrons decay as fast as the luminescence, thus dominating the first part of the upconversion decay. Once the initial electrons are exhausted, only upconversion from the remaining traps can occur. This upconversion decays slowly following the decay of the IR absorption centers. A conclusion is that the IR absorption traps, although dominated in their decay by non-visible-luminescent transitions, are still able to supply electrons for upconversion.

It is evident, at this point, that the energy scheme described in Section 2.1 and illustrated in Fig. 1 is oversimplified. But the information available is not sufficient to propose a more realistic one. Continuation of this work, in order to clarify the energy scheme and understand the origin and the role of the non-radiative transitions, would be very useful since it could lead to a control of the processes that directly determine the internal quantum efficiency.

In Fig. 16 the temperature dependence of the intensity of the upconversion emission is presented. It is seen that upconversion is extremely sensitive to temperature. It has totally disappeared by 40°K.

The decrease of the upconversion effect, as the temperature increases, is due to thermal release of trapped electrons. The only available estimated value of the impurity depth is of the order of 0.07 eV from the conduction band.[5] For such a depth the overlapping at the Fermi function with the conduction band is almost negligible at 40°K. However, the electron

densities depend on the product of the Fermi function and the density of states. The low density of traps compensates the low value of the Fermi function at the conduction band. It is expected that if the number of upconversion traps is increased, the upconversion effect will still be appreciable at higher temperatures. In fact, since the total density of IR absorption centers is much larger than the effective upconversion centers, UV-induced IR absorption was observed at temperatures as high as 270°K.

2.5 Conclusions and Recommendations

The chemical vapor deposition (CVD) technique was used to grow thick single crystal films of epitaxial ZnS on GaAs or ZnS substrates. By a feedback mode of operation between crystal growth and optical evaluation, it was possible to develop an effective doping technique. ZnS substrates were used for the final upconversion films, since it was demonstrated that GaAs substrates and ZnS films dope each other with Zn and Ga. The films were doped with Cu as activator. Cl instead of Al was chosen as co-activator since it was easier to transport and was already present in the CuCl used to transport Cu.

Epitaxial films were obtained which exhibited the green luminescence at 5230 Å and the blue self-activated luminescence at 4520 Å. When illuminated with IR radiation, IR stimulated luminescence (upconversion emission) was observed. With an intense IR source the effect was visible with the eye.

For the first time it was possible to obtain the spectral dependence of the upconversion emission, showing that its spectrum is nearly identical to that of the luminescence. This proved that in the upconversion process electrons were excited into the conduction band rather than experience resonant tunnelling.

The UV induced IR absorption was large, with absorption coefficients of the order of 800 cm^{-1}. Study of transient effects indicated that a strong non-visible-luminescent mechanism was present and supplied the principal recombination path for the IR absorbing centers.

Presumably, because of such competing decay mechanisms, the internal quantum efficiency, defined as the ratio of the number of emitted visible photons to the number of IR absorbed photons, was low. The best measured value was 10^{-4}. In some samples it may have been larger, but 10^{-3} is considered as the upper limit.

From this study, the following practical conclusions are derived:

1. CVD can be successfully used to grow epitaxial films suitable for upconversion. The advantage that CVD has over bulk growth is fast production of crystals and fine control of doping. This leads to fast iteration in the process of material optimization.
2. The upconversion efficiency of CVD-grown films is of the same order as that reported for bulk-grown crystals. Optimization of doping concentrations would presumably lead to some increase in the present ceiling of 10^{-3} for the internal quantum efficiencies.
3. These results indicate that a large IR absorption, not leading to visible-luminescent transitions, is competing with the upconversion effect and is responsible for the low efficiency. It is believed that more investigation with these techniques would shed light on the competing mechanism. Only after this mechanism is clarified will it be possible to determine rationally the maximum expectable quantum efficiency.

3.0 HETEROJUNCTION UPCONVERTER REPORT

3.1 INTRODUCTION

In the introduction an alternative approach to upconvert IR radiation was briefly mentioned. The motivation for searching for an alternative approach stems from two basic major drawbacks of the phosphor upconverters. 1) The absorption of IR leading to upconversion is small -- this is a fundamental limitation resulting from the fact that the mechanism is proportional to the density of active impurities. 2) The device requires stimulation from an external UV source.

A device which does not suffer from the above fundamental drawbacks is a graded heterojunction structure. In this approach IR is absorbed in a small bandgap material creating electron-hole pairs. A bias potential across the structure transports the photo-excited electrons to a region of the semiconductor with larger bandgap where they recombine. In principle this simple concept avoids the pitfalls of the phosphor mentioned earlier. However, the efficiency now is limited by the transport and recombination processes.

A heterojunction structure which gives extremely high efficiency and low bias current is shown in Fig. 17. The structure is basically of a p-n-p^+ type, somewhat analogous to a PNP transistor (with the collector at the left) operating in a "punched-through" mode. The region between the absorbing p layer and recombining p^+ layer is of a larger bandgap than either of the p-layers and is completely depleted by the applied reverse bias on the left junction plus the built-in voltage on the right junction.

In fact, the bias is increased beyond the point of complete depletion to the point where the potential "hump" in the valence band is reduced till it just holds off the hole current. As seen in Fig. 17, if the energy gap in this layer is graded as shown, the conduction band potential will indeed be steadily decreasing from the absorbing region to the emitting region under this bias. Hence, electrons photogenerated by IR absorption in this layer will in principal be efficiently transported to the wide bandgap p^+ layer for efficient radiative recombination.

This device can be operated in either a reflective mode where the IR input light would be incident from the right, or in the transmissive mode from the left, as shown in Fig. 17. In the transmissive mode, the light would be incident through an IR-transparent substrate and the absorbing layer would have a thickness of the order of a diffusion length for electrons. Another optional feature is the use of a wider bandgap surface contact layer to confine the photogenerated carriers to a thin recombination region and avoiding possible re-absorption of the visible emitted light.

3.2 TECHNICAL APPROACH

3.2.1 Introduction

In this initial study we focused on the alloys of $InAs_{1-x}P_x$. This material is not suitable for application at 10μ; however, some fundamental aspects of the device such as the efficient transport across the heterojunction can be elucidated. Even though the choice of these alloys was principally dictated from considerations of time and simplicity, an efficient device at 3μ would be of great interest.

3.2.2 Crystal Growth

Since the chemical vapor deposition (CVD) crystal-growth technique offers a versatile technique of grading $InAs_xP_{1-x}$, such a technique was used to grow the epitaxial layers. The reactor system is shown in Fig. 18. This reactor has the capability of grading the composition continuously by varying the arsine (AsH_3) and phosphine (PH_3) gases during the crystal growth. The variation is done externally using a Data-Track programmer to control the flow rate of the gases.

As a result of intensive studies on the growth of high quality $InAs_xP_{1-x}$ films, it was found that for optimum conditions the gases and their flows for $x = C.45$ are:

1. Arsine 3.5 cc/min
2. Phosphine, 20 cc/min
3. Hydrogen used as carrier gas for arsine and phosphine, 800 cc/min
4. HCl gas for metal indium, 2.5 cc/min and carrier gas (H_2) 275 cc/min.

The substrate temperature was at 665°C. The optimum transport rate for indium was found to be about $1x10^{-4}$ moles/min. Typical growth rate was about 6μ/hr. The quality and smoothness of these films far exceeds those reported in the literature. The principal reason for this success is the ability to determine the optimum condition for the zone of deposition and the flow conditions as discussed in Section 2.1 in this report.

3.3 RESULTS AND DISCUSSION

3.3.1 Material

$InAs_xP_{1-x}$ epitaxial films of different composition have been grown on p-type as well as undoped InAs substrates. These substrates were obtained from Electronic Materials Corporation.

Figure 19 shows the quality of the epitaxial films which were grown. The substrate used was the (111) plane of InAs. From the figure, it can be seen that the interface is very well defined and the layer is very smooth (a mirror finish). The film thickness is about 9.5μ. Figure 20 shows the Laue pattern of this film. The Laue pattern reveals a three-fold symmetry of the (111)-plane and also the crystallinity by the brightness of the spots.

The composition of the alloy was determined using the Bond spectrometer. The accuracy in determining the alloy via the lattice constants was better than 0.1%.

The optimum growth rate was about 5μ/hr to give a smooth surface (as shown in Fig. 19). Faster growth rates were attempted, but the surface became rougher.

3.3.2 Electrical Measurements

Electrical measurements on the grown epi-layers of $InAs_xP_{1-x}$ on various undoped and p-type InAs substrates show that the electron mobility ranges from 30,000 cm^2/v-sec to about 5,000 cm^2/v-sec at room temperature and the carrier concentration ranges from 10^{17} to 10^{19} cm^{-3}. It is believed that the reason for this naturally-grown n-type is sulphur in the indium metal. Although purification of the indium metal was attempted, reduction

of the carrier concentration further to 10^{15} cm^{-3} was not successful. However, an improvement from 10^{19} to 10^{17} cm^{-3} was achieved. Further reduction in the carrier concentration has to come from purifying the hydrogen carrier gas or by lowering the growth temperature. Fig. 21 shows the typical results of the electron mobility as a function of composition for room temperature (300°K) as well as at liquid nitrogen temperature (77°K). This Hall measurement was done using the Van Der Pauw technique.

Fig. 22 shows the V-I characteristic of a diode at 77°K. The diode was fabricated in mesa form. Fig. 22a shows the ungraded characteristic of an $InAs_{0.45}P_{0.55}$ film. The substrate is a p-type (111) plane of InAs. Fig. 22b shows the characteristic of a graded $InAs_{0.45}P_{0.55}$ film. Since the naturally-grown alloy is n-type, no attempt was made to dope these films.

3.3.3 Optical Measurements

The optical measurements were performed using a modified Beckman spectrometer (Model ID4). The grown layer of the alloy was $InAs_{0.45}P_{0.55}$. The thickness of these films was about 3μ. Fig. 23 shows the photoresponse of the graded and ungraded InAsP. The substrate used to grow the layers was the (111)-plane of p-type InAs. The lattice mismatch between the film and the substrate is about 1.6%. This measurement was done at liquid nitrogen temperature (77°K) in a dewar (manufactured by Cryogenic Associates) with ZnS material as the window. It is obvious from the result that the graded alloy has a better photoresponse than the ungraded one. Since the spectrometer cut-off is at 2μ, the shorter wavelength response was not measured. However, the interesting result is near 3μ region,

since the bandgap of InAs at 77°K is about 0.404 eV corresponding to a wavelength of 3.06μ. A comparison of the photoresponse for a graded and ungraded structure suggests that the former structure leads to better transport properties. These results point to the fact that photo-excited electrons created in InAs by bandgap radiation can be transported across the metallurgical junction. The efficiency of this process is crucial in this device concept.

3.4 CONCLUSION AND RECOMMENDATIONS

In a short period of six-months some of the properties of $InAs_{1-x}P_x$ epilayers on InAs have been elucidated. Films of high optical quality for different values of x have been grown. The CVD system is capable of automatically grading the alloy with a lattice mismatch not exceeding 2% between the epilayer and the substrate. The preliminary results of photo-response indicate that the graded structure does not impede the transport of carriers across the metallurgical junction. The electron mobility of these alloyed films is comparable to the bulk value.

Although the alloys of InAsP can only be used to upconvert wavelengths shorter than 3μ and hence are not adaptable to the imaging requirements at 10μ, our results indicate that the system is well worth further study for shorter wavelength applications.

4.0 REFERENCES

1. Alan G. Becker and Q Risgin, "The Feasibility of a Zinc Sulfide Up-Converter for Infrared-Red Imaging," ECOM-00013-0030-F.
2. W. J. Scouler, O. H. Dickey, and T. M. Quist, "Experimental Evaluation of Upconversion in ZnS as a Potential IR Imaging Device," paper presented at the 19th National Infrared Information Symposium (June 1971).
3. W. J. Scouler, D. H. Dickey, T. M. Quist, and R. J. Keyes, "Experimental Evaluation of Upconversion in Zinc Sulfide as an IR Imaging Device," presented at IRIS Spec. Group on Imaging. See also, Optics Research 2, 47 (1971).
4. See, for example, Physics and Chemistry of II-VI Compounds, edited by R. Aven and J. S. Prener, North-Holland Publishing Company, Amsterdam, 1967.
5. H. Kukimoto, S. Shionoya, T. Koda, and R. Hioki, J. Phys. Chem. Solids 29, 935 (1968).
6. K. Urabe and S. Shionoya, J. Phys. Soc. Japan 24, 543 (1968).
7. K. Era, S. Shionoya, Y. Washizawa, and H. Ohmatsu, J. Phys. Chem. Solids 29, 1843 (1968).
8. W. M. Yin and E. J. Stofko, "Vapor-Phase Epitaxial Growth and Some Properties of ZnSe, ZnS and CdS," J. Electrochem. Soc. 119, 381 (1972).
9. D. G. Thomas, J. J. Hopfield, and W. M. Augustyniak, Phys. Rev. 140, A202 (1965).

5.0 PUBLICATIONS

As a result of this work we are preparing several papers for publication. The new information is in the areas of (1) crystal growth and dopant studies, (2) mechanisms of upconversion, and (3) properties of graded heterostructures of $InAs_{1-x}P_x$.

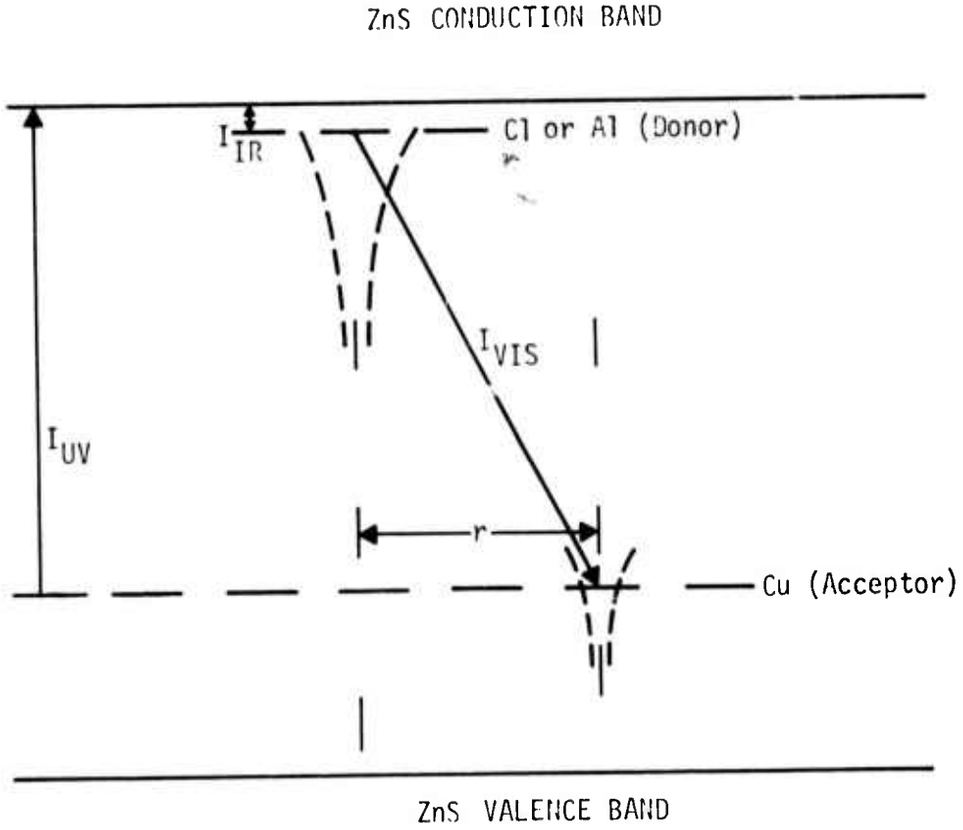
ZnS CONDUCTION BAND
I_{IR}
Cl or Al (Donor)
I_{VIS}
I_{UV}
r
Cu (Acceptor)
ZnS VALENCE BAND

Figure 1

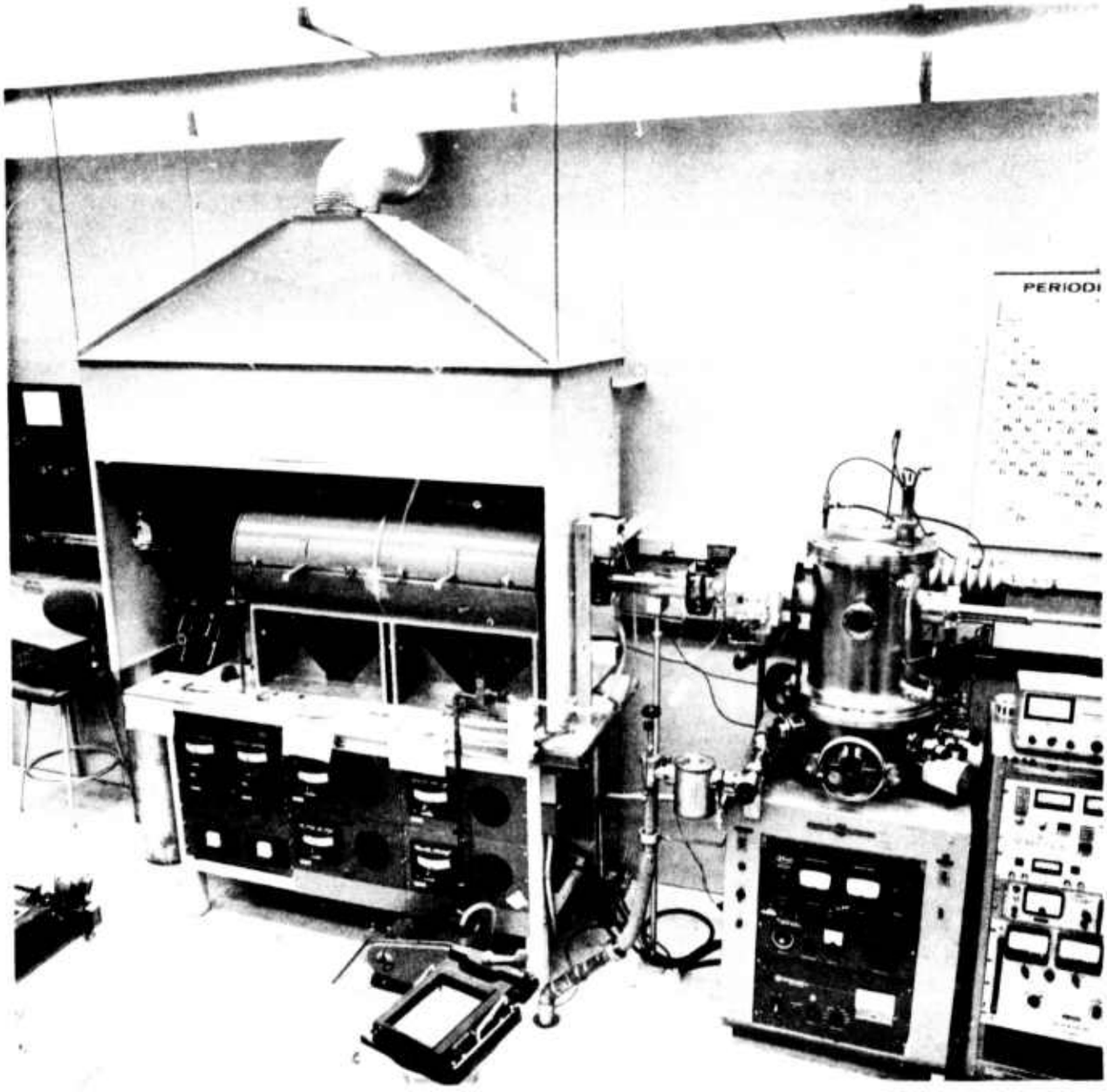

Figure 2

THE CHEMICAL VAPOR DEPOSITION REACTOR

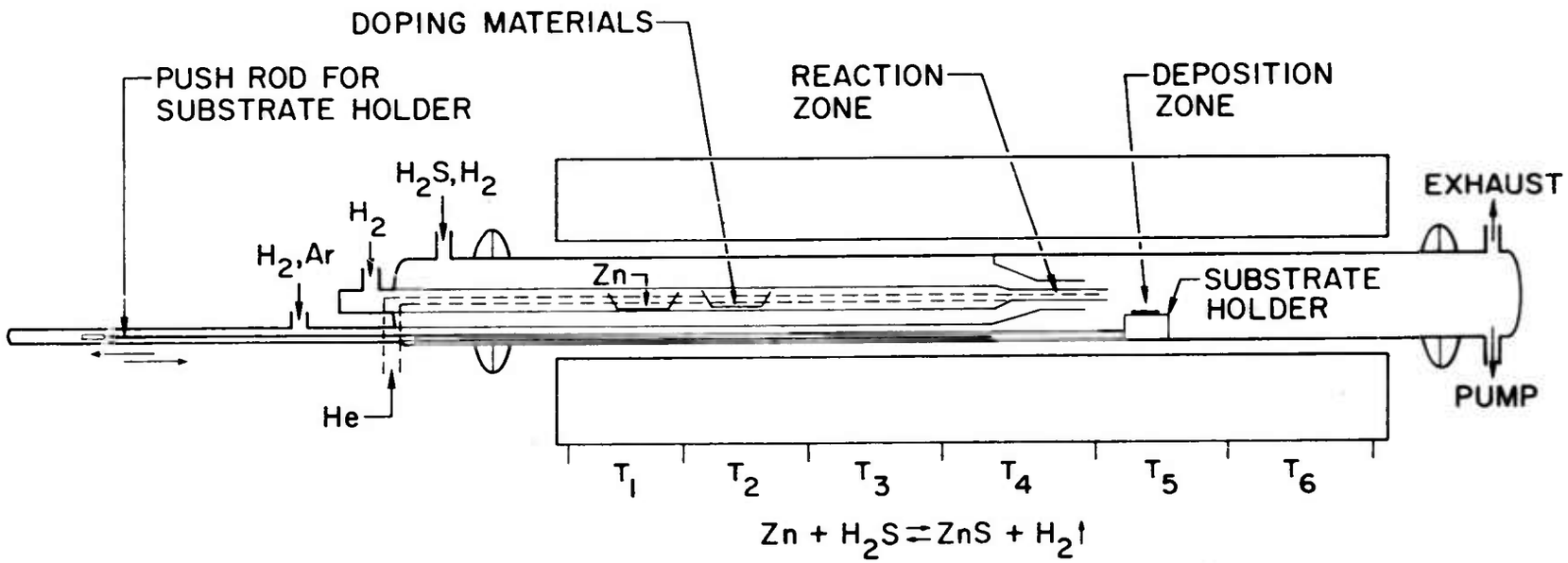

Figure 3

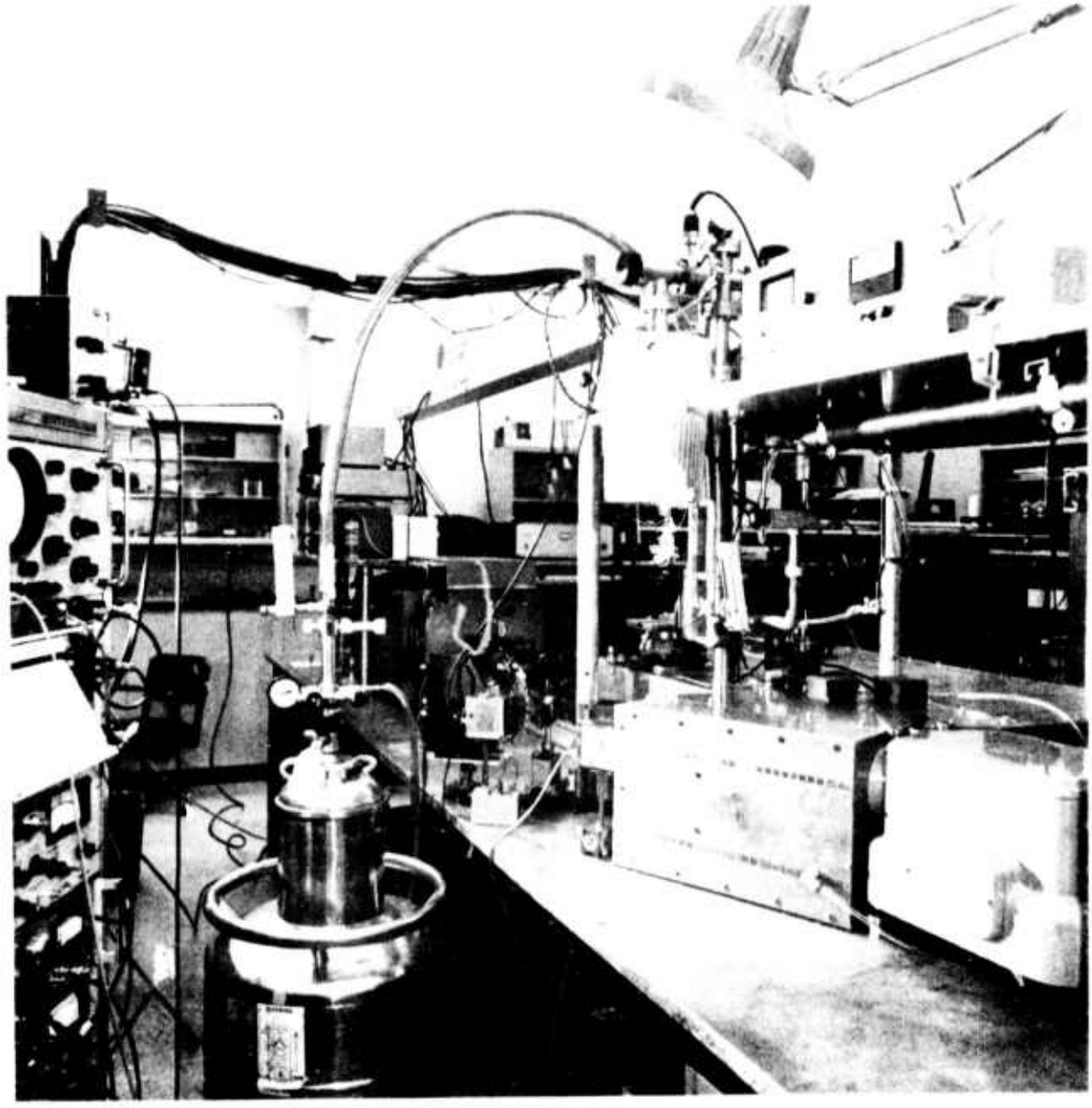

Figure 4

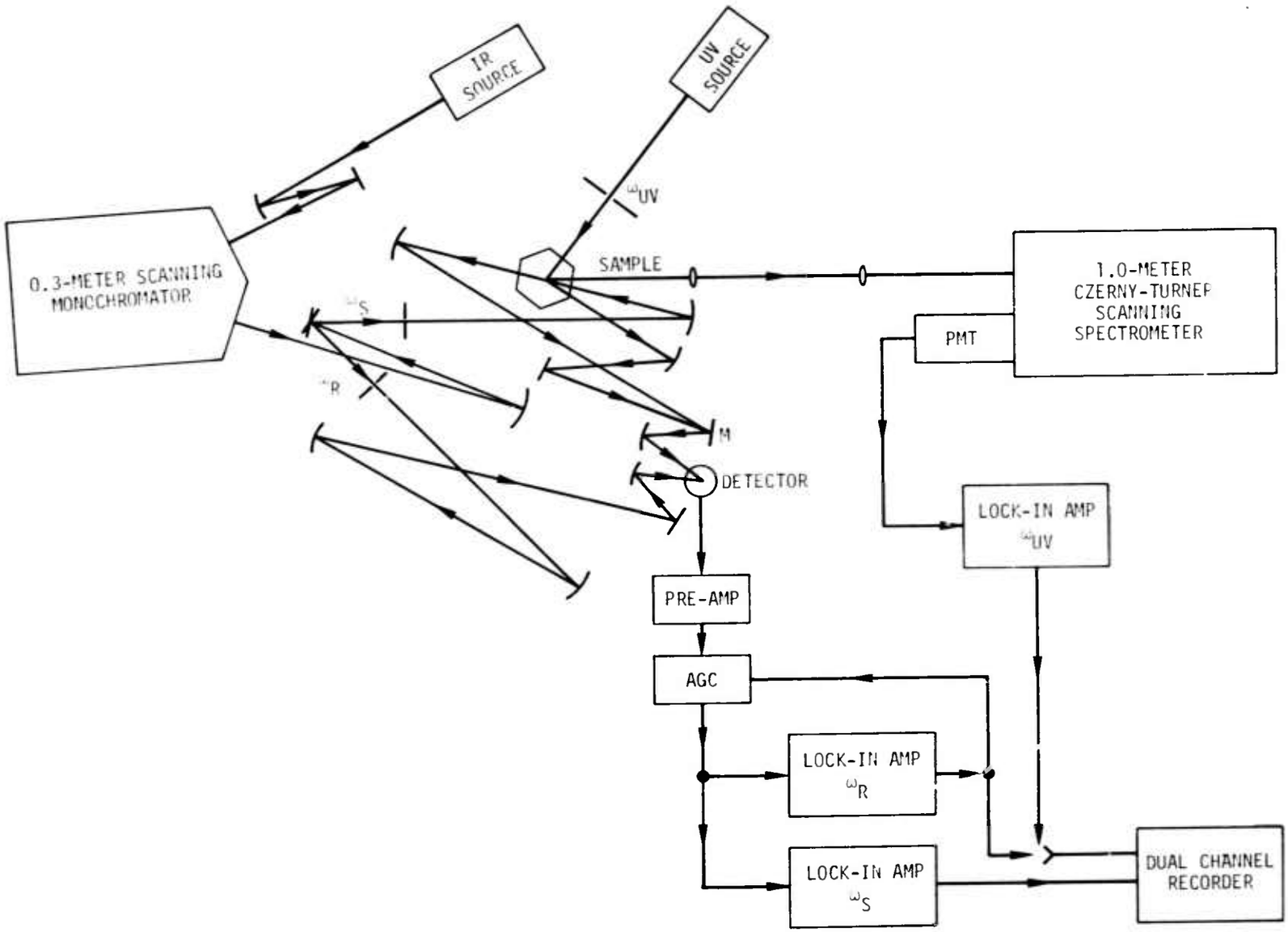
IR SOURCE
UV SOURCE
ω_{UV}
0.3-METER SCANNING MONOCHROMATOR
SAMPLE
1.0-METER CZERNY-TURNER SCANNING SPECTROMETER
PMT
ω_S
ω_R
M
DETECTOR
LOCK-IN AMP ω_{UV}
PRE-AMP
AGC
LOCK-IN AMP ω_R
LOCK-IN AMP ω_S
DUAL CHANNEL RECORDER

Figure 5

DIFFRACTOMETER OUTPUT OF THE β-ZnS FILM
GROWN ON THE (100) PLANE OF GaAs

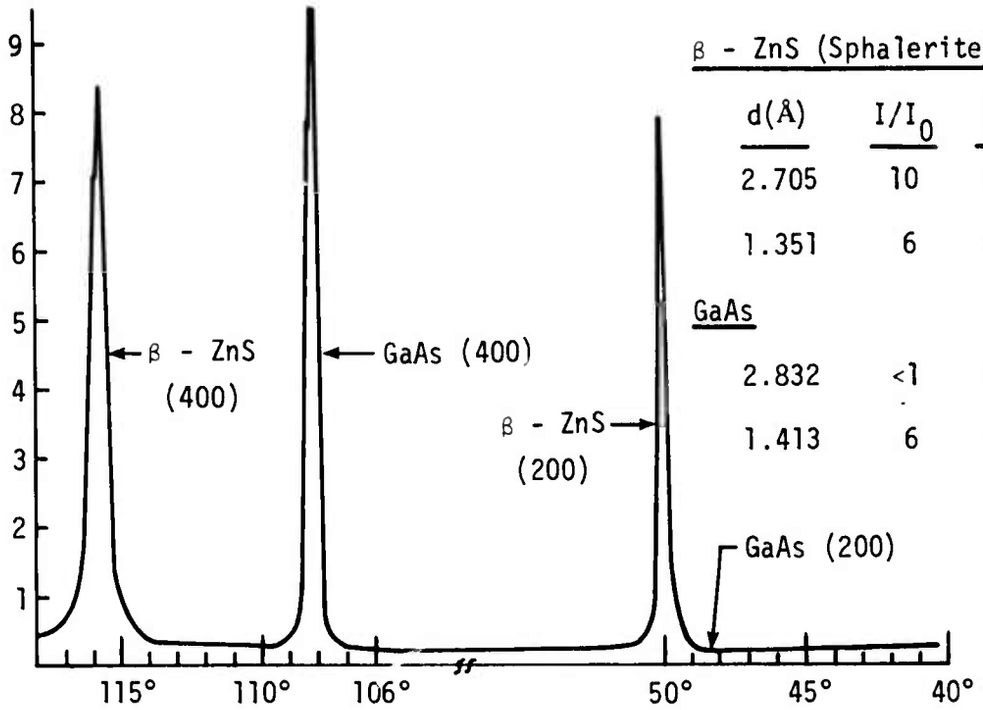

β - ZnS (Sphalerite)

d(Å)	I/I_0	hkl	2θ
2.705	10	200	50.1°
1.351	6	400	115.86°

GaAs

2.832	<1	200	47.68
1.413	6	400	108.24°

Figure 6

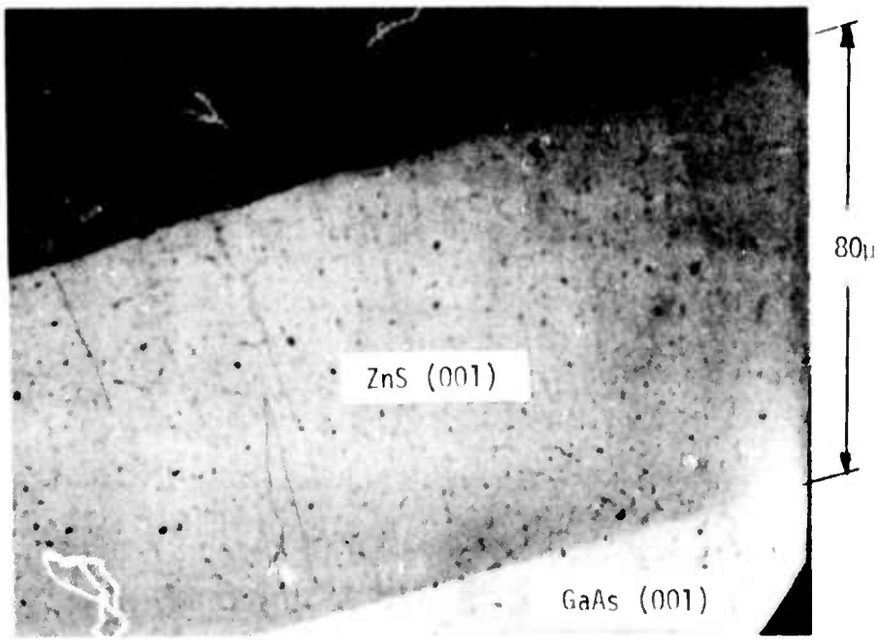

Figure 7a

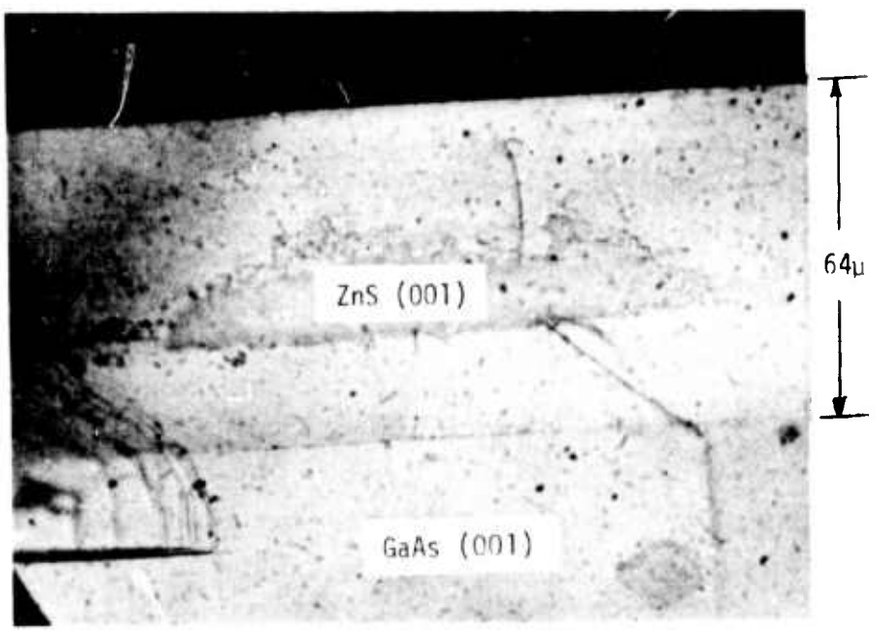

Figure 7b

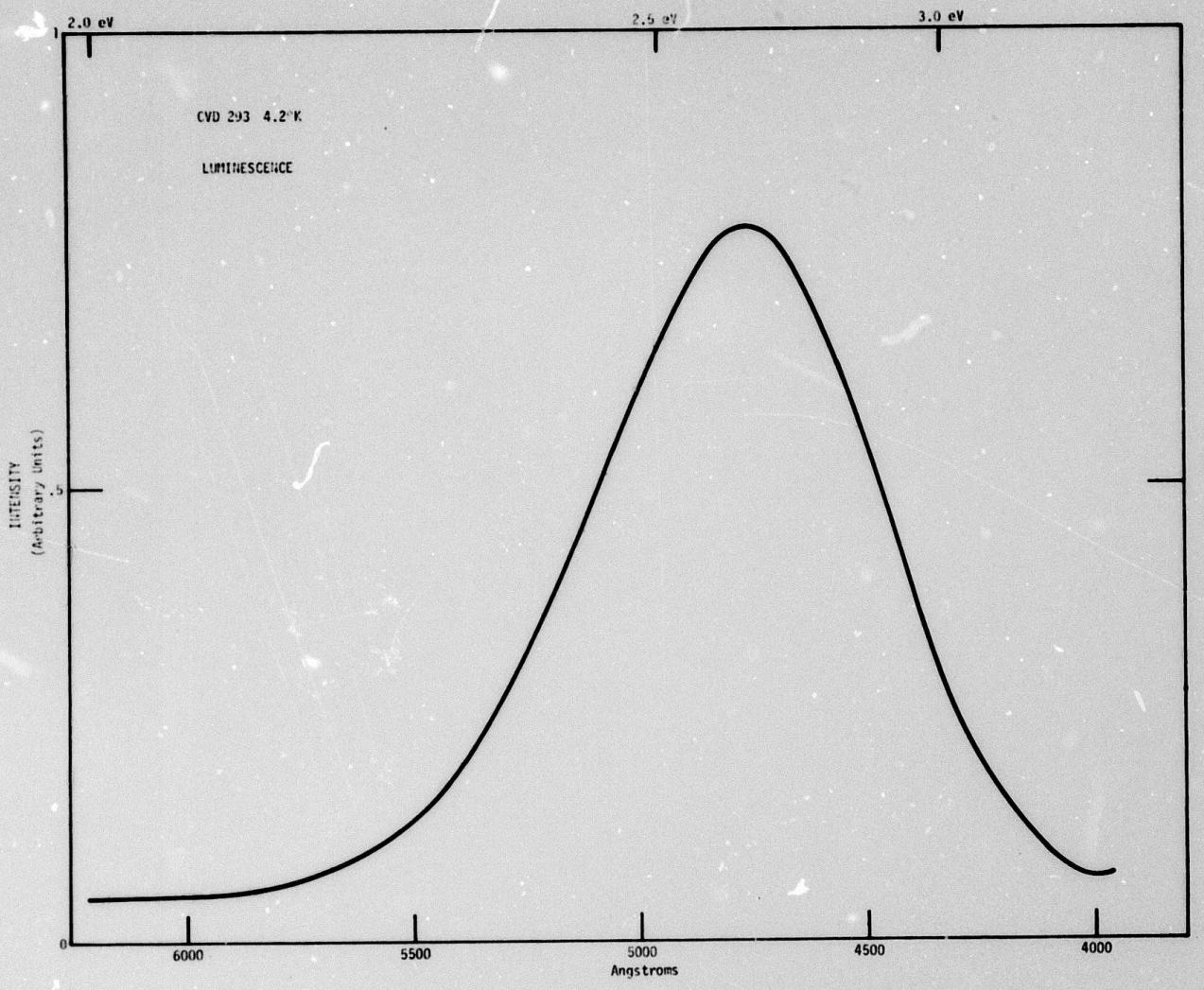
2.0 eV
2.5 eV
3.0 eV
CVD 293 4.2°K
LUMINESCENCE
INTENSITY
(Arbitrary Units)
1
.5
0
6000
5500
5000
4500
4000
Angstroms

Figure 8

Figure 9a

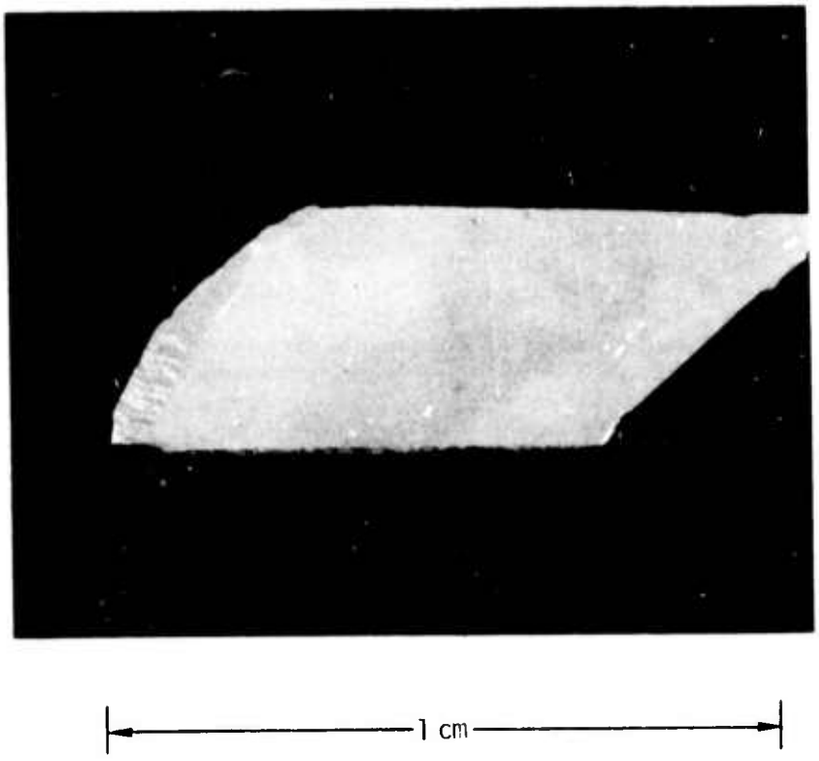

Figure 9b

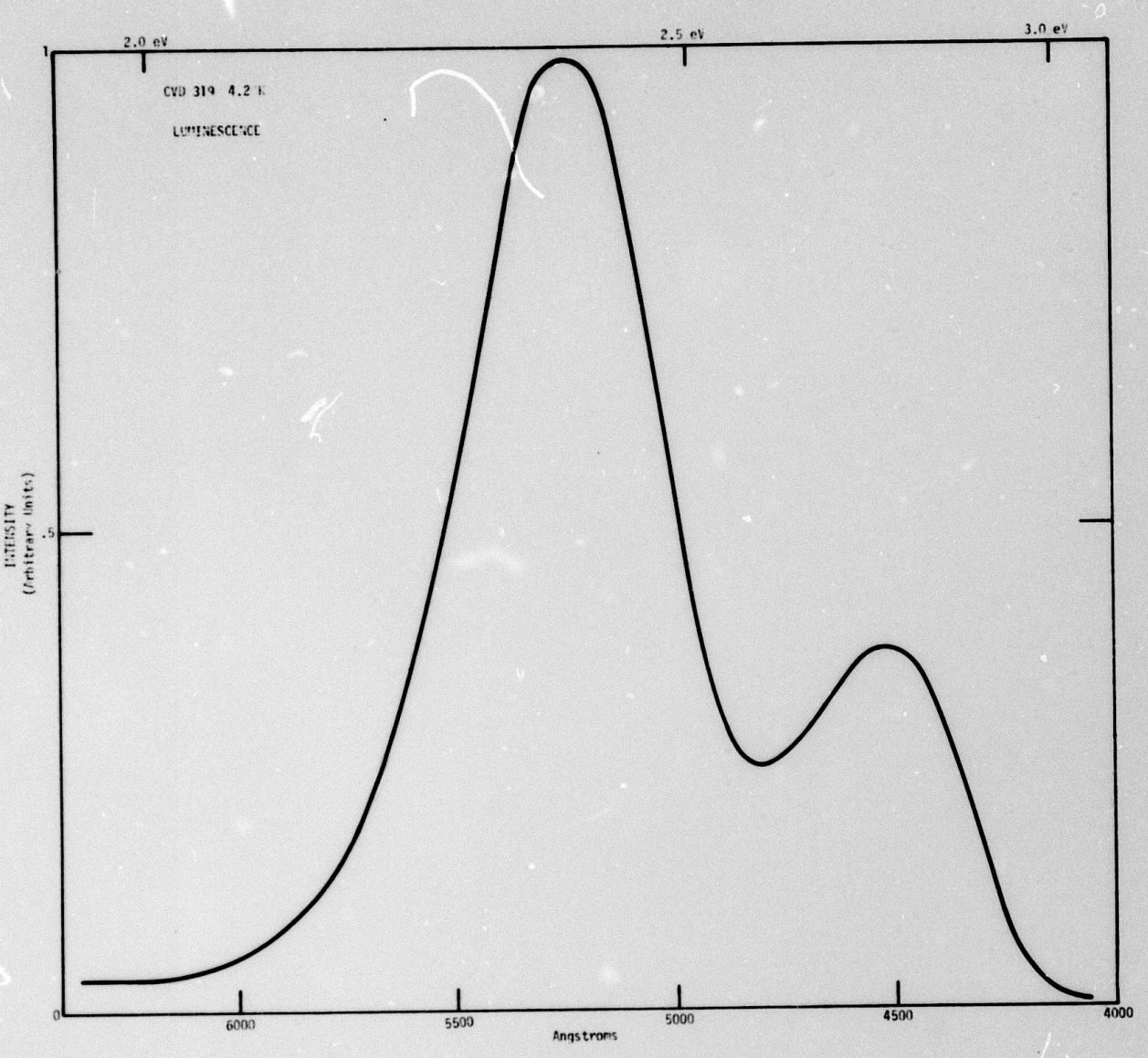
2.0 eV
2.5 eV
3.0 eV
CVD 319 4.2 K
LUMINESCENCE
INTENSITY
(Arbitrary Units)
1
.5
0
6000
5500
5000
4500
4000
Angstroms

Figure 10

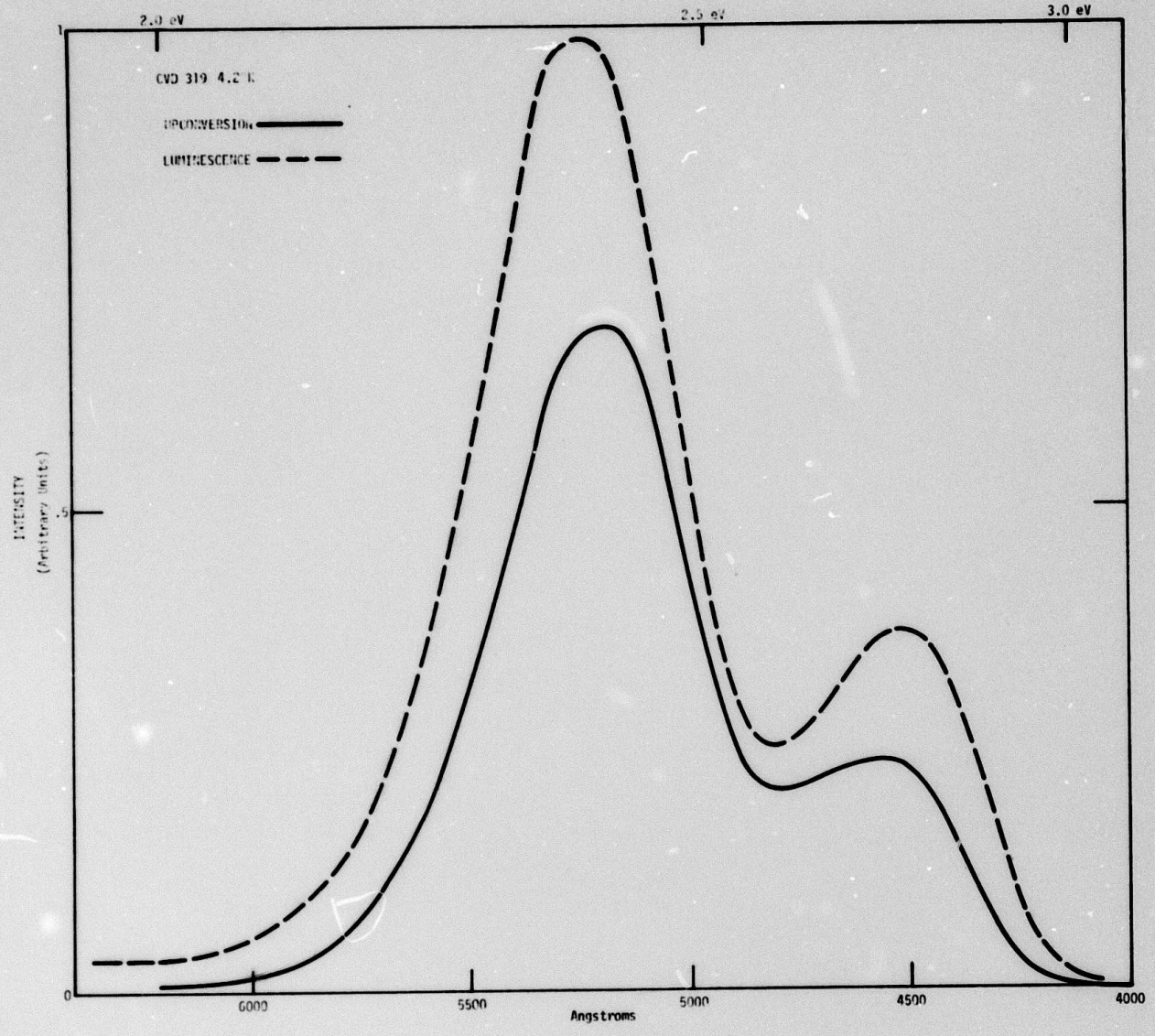
2.0 eV
2.5 eV
3.0 eV
CVD 319 4.2 K
PHOTOCONVERSION
LUMINESCENCE
INTENSITY
(Arbitrary Units)
1
.5
0
6000
5500
5000
4500
4000
Angstroms

Figure 11

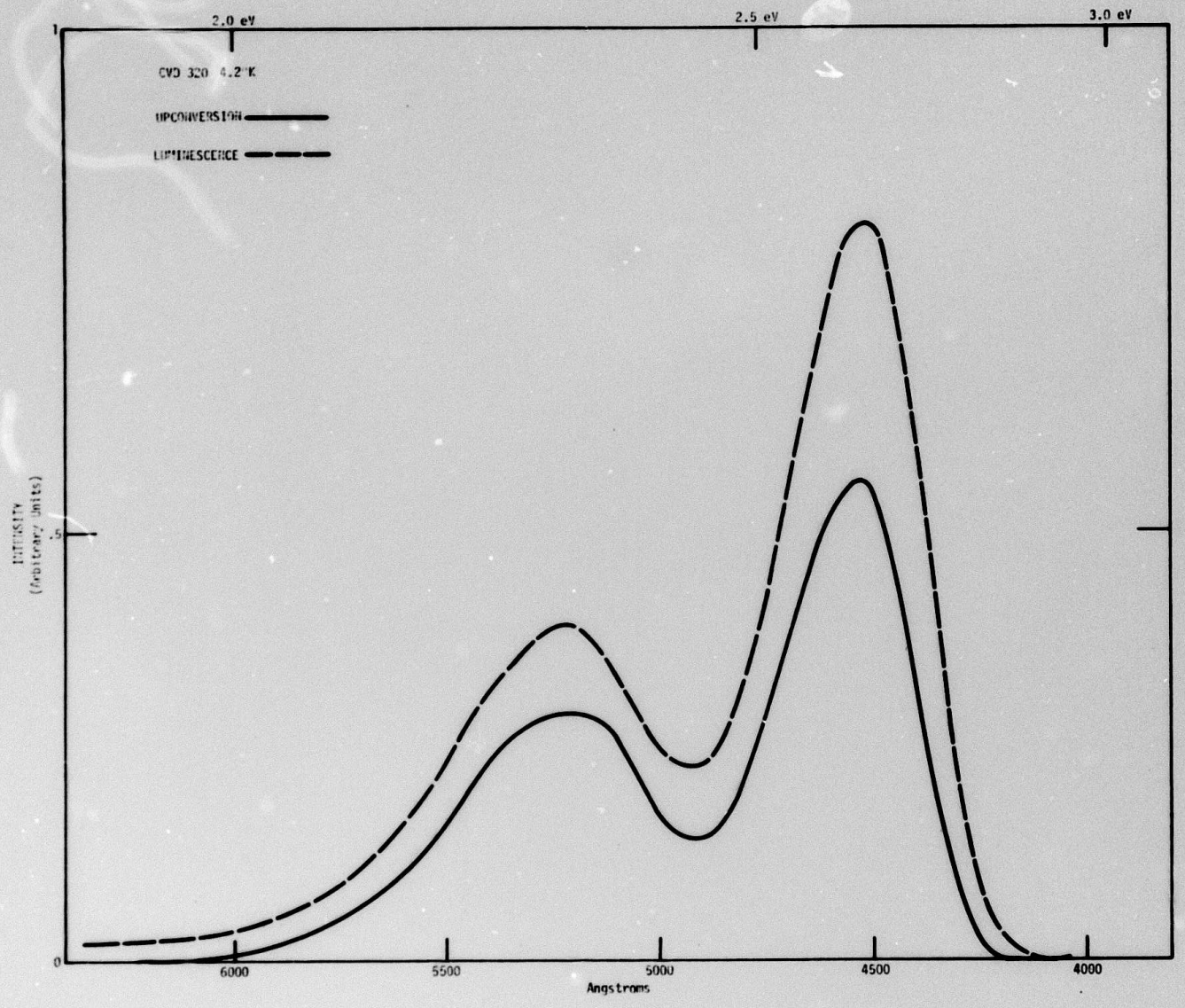
2.0 eV
2.5 eV
3.0 eV
1
.5
0
CVD 320 4.2°K
UPCONVERSION
LUMINESCENCE
INTENSITY
(Arbitrary Units)
6000
5500
5000
4500
4000
Angstroms

Figure 12

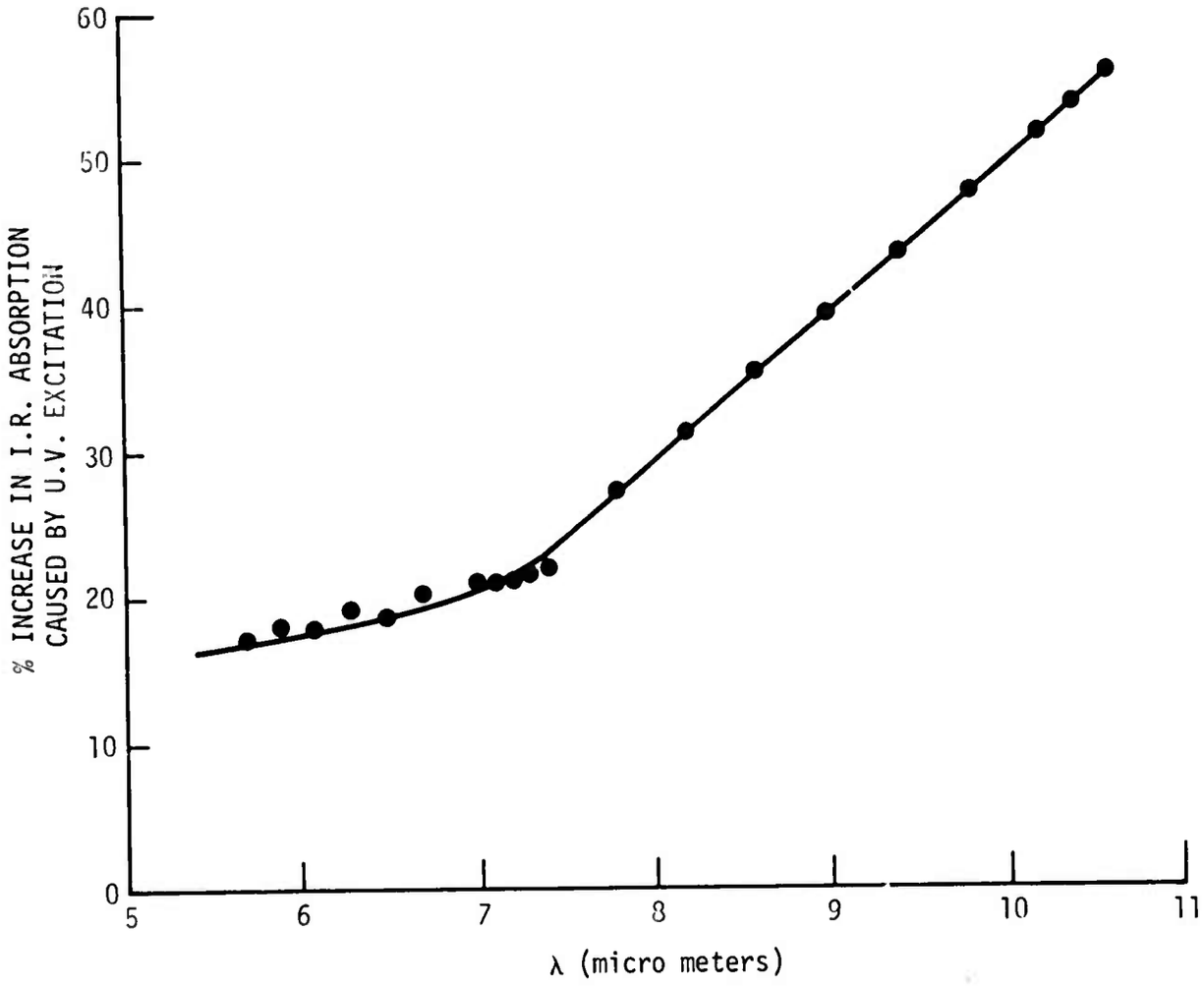
% INCREASE IN I.R. ABSORPTION
CAUSED BY U.V. EXCITATION
60
50
40
30
20
10
0
5
6
7
8
9
10
11
λ (micro meters)

Figure 13

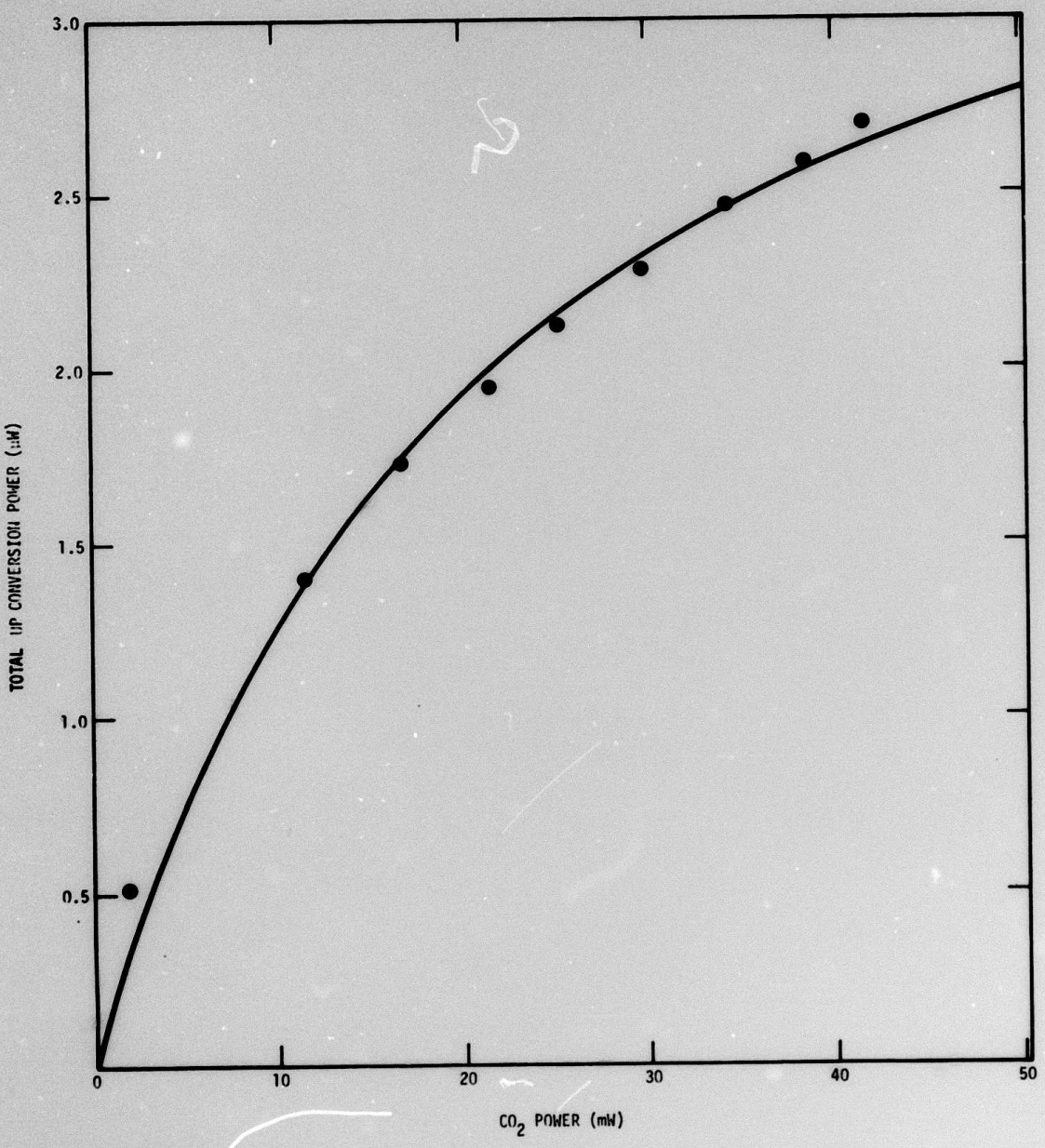
TOTAL UP CONVERSION POWER (μW)
3.0
2.5
2.0
1.5
1.0
0.5
0
10
20
30
40
50
CO_2 POWER (mW)

Figure 14

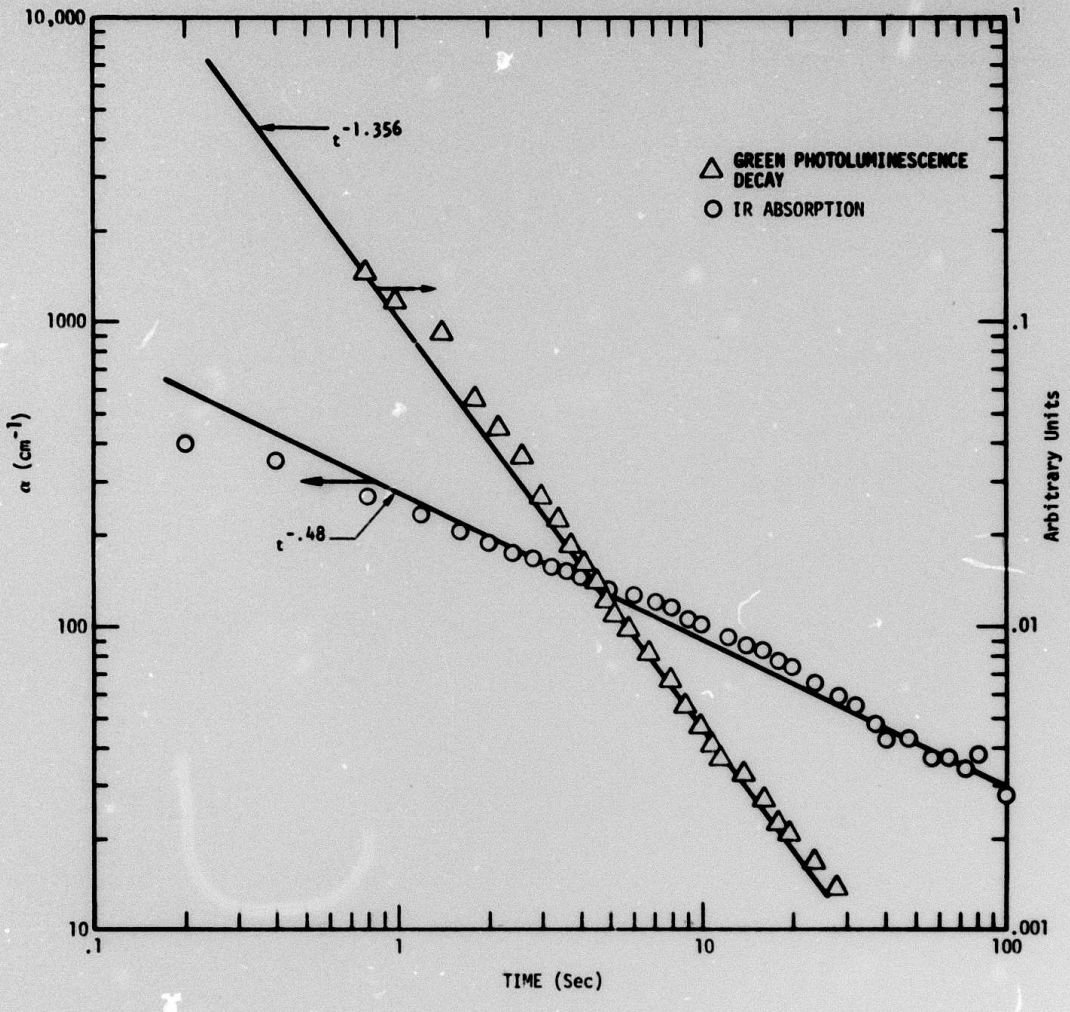
10,000
1000
100
10
.1
1
10
100
1
.1
.01
.001
α (cm⁻¹)
Arbitrary Units
TIME (Sec)
t^-1.356
t^-.48
GREEN PHOTOLUMINESCENCE DECAY
IR ABSORPTION

Figure 15a

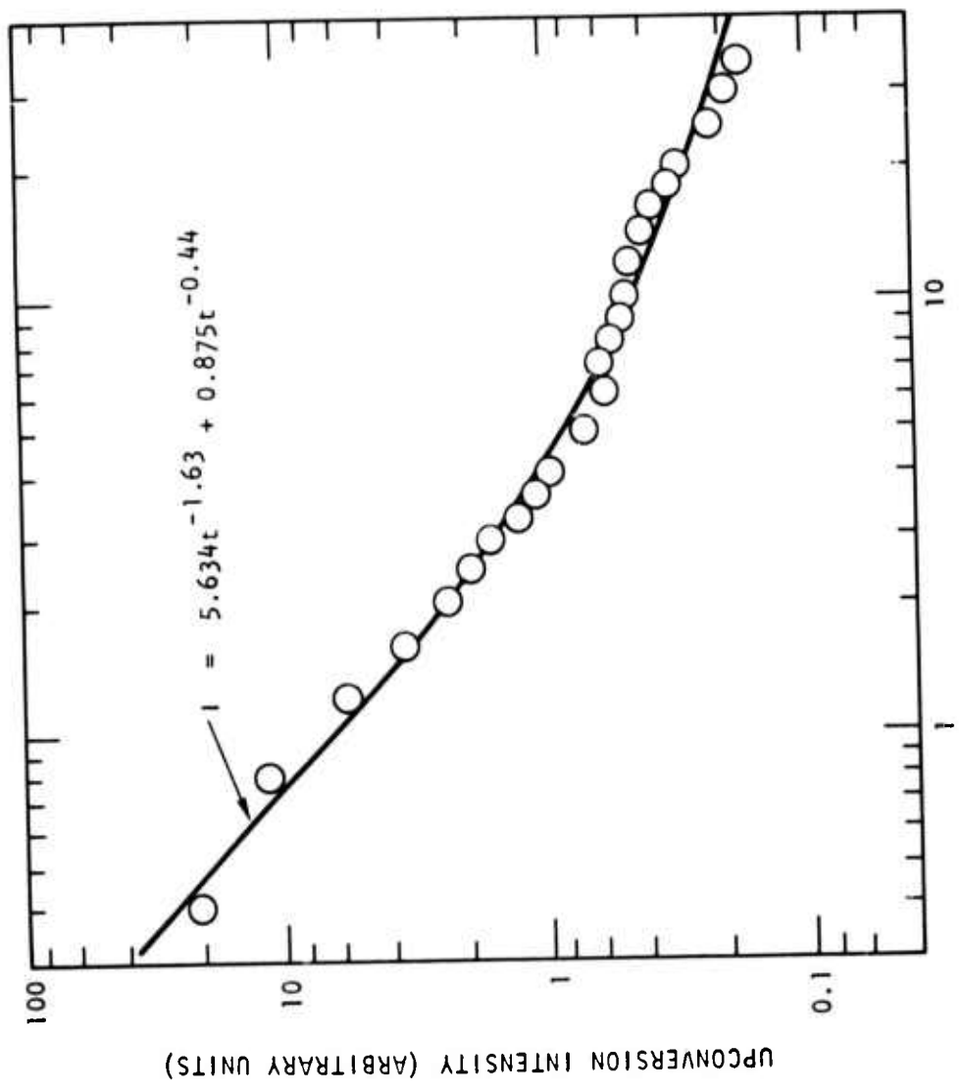
$I = 5.634t^{-1.63} + 0.875t^{-0.44}$
100
10
1
0.1
1
10
TIME (sec)
UPCONVERSION INTENSITY (ARBITRARY UNITS)

Figure 15b

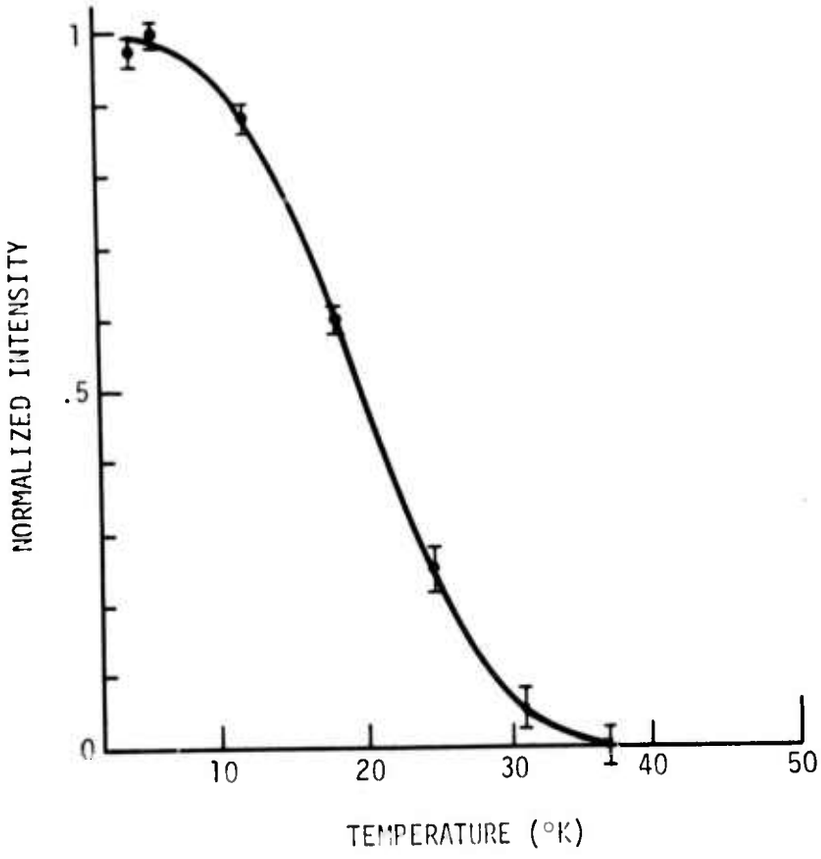

Figure 16

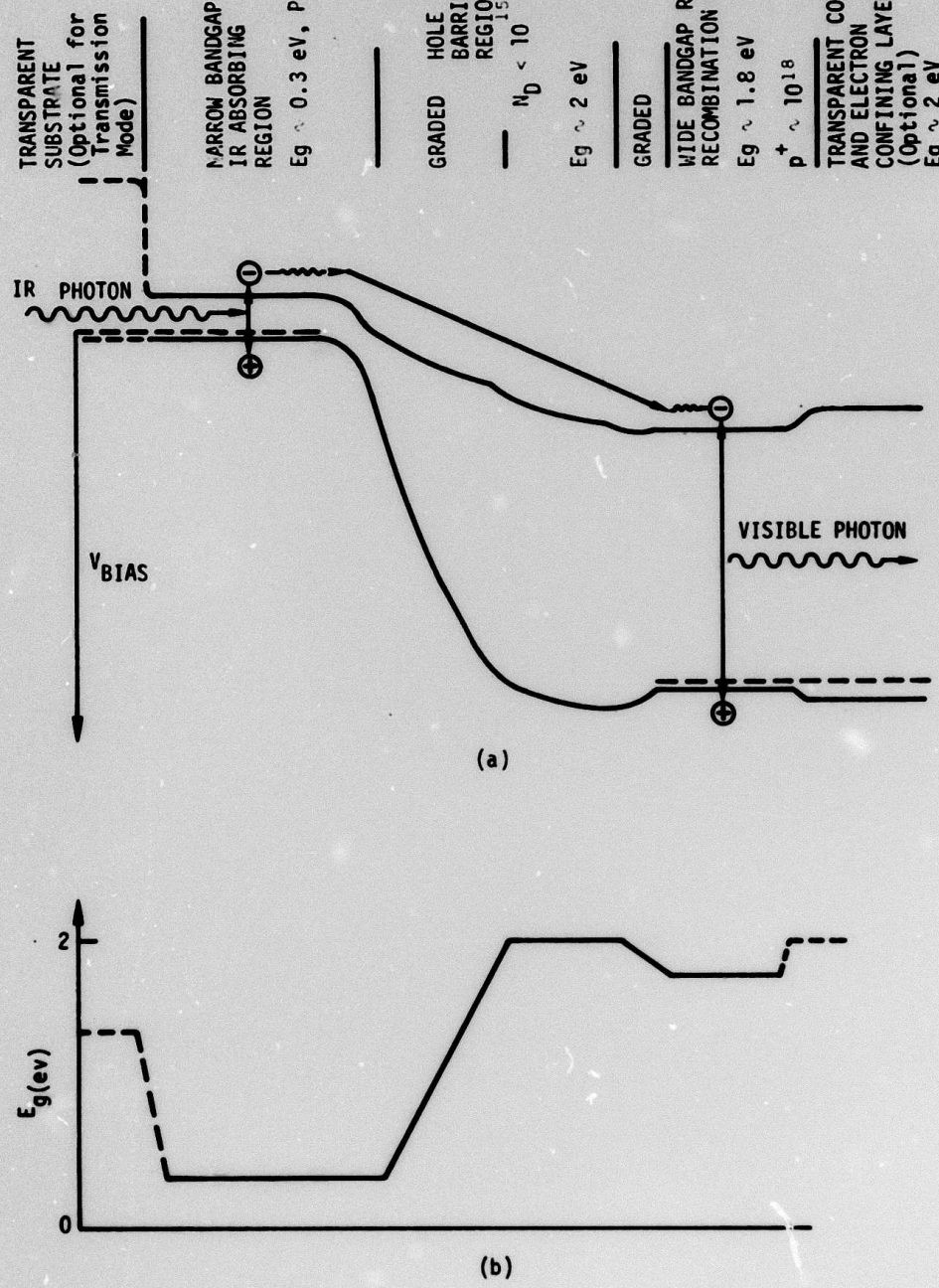
TRANSPARENT SUBSTRATE (Optional for Transmission Mode)
NARROW BANDGAP IR ABSORBING REGION
Eg ~ 0.3 eV, P-type
GRADED
HOLE BARRIER REGION
$N_D < 10^{15}$ cm^{-3}
Eg ~ 2 eV
GRADED
WIDE BANDGAP RADIATIVE RECOMBINATION REGION
Eg ~ 1.8 eV
$p^+ \sim 10^{18}$
TRANSPARENT CONTACT AND ELECTRON CONFINING LAYER (Optional)
Eg ~ 2 eV
P ~ 10^{16}
IR PHOTON
VISIBLE PHOTON
V_{BIAS}
(a)
2
$E_{g(ev)}$
0
(b)

Figure 17

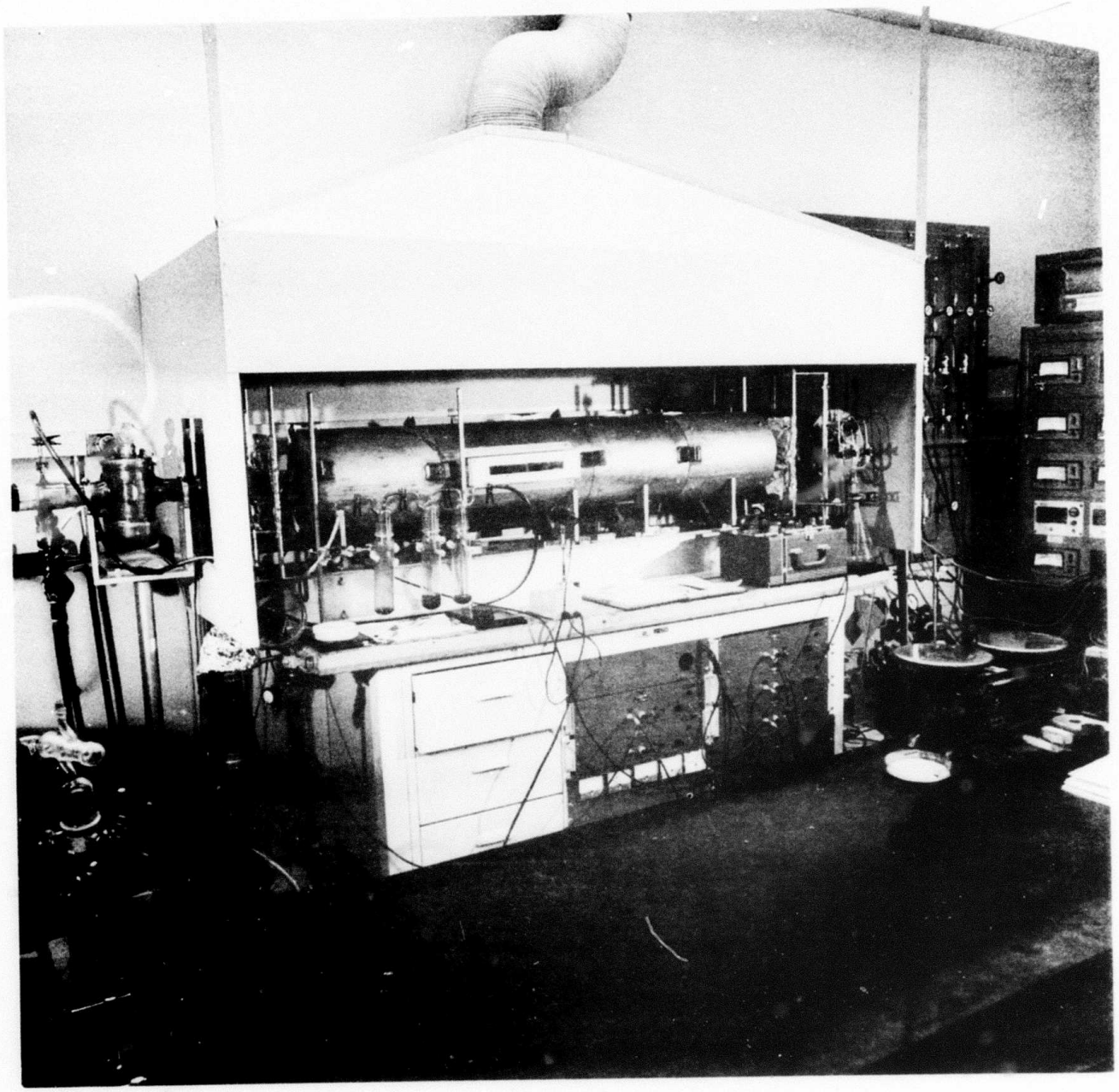

Figure 18

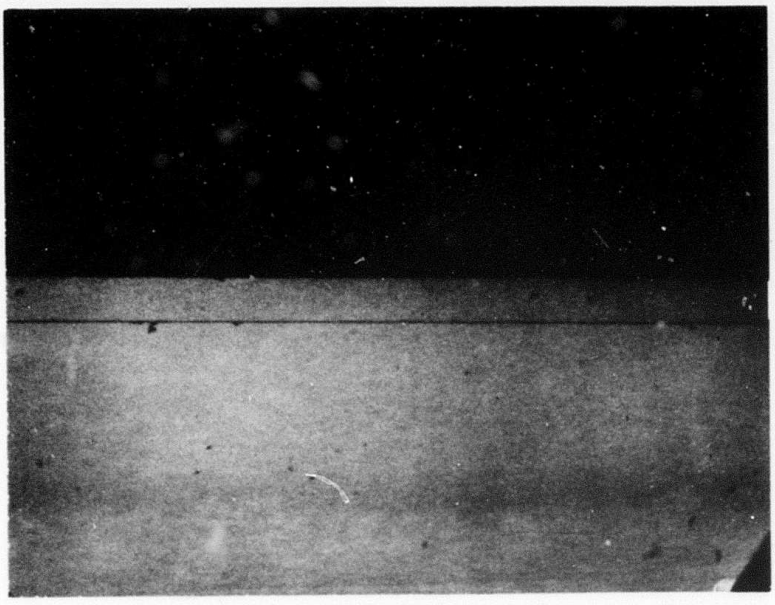

Figure 19

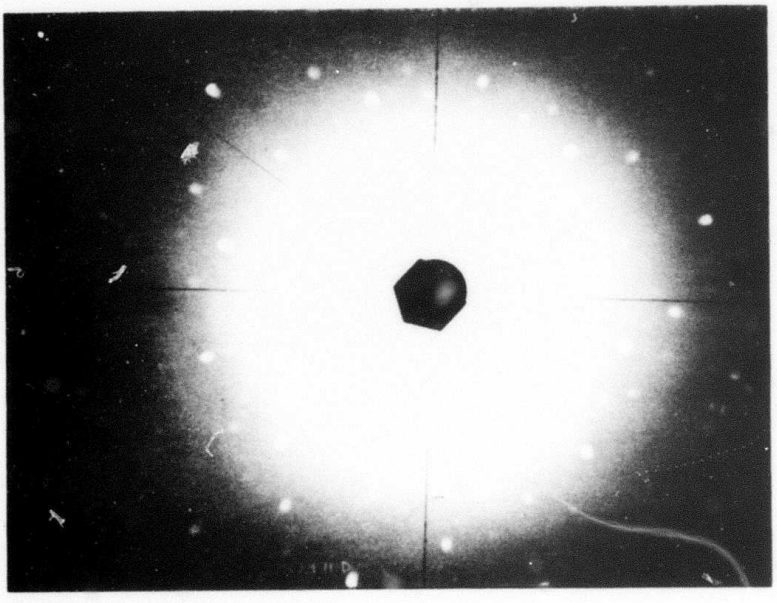

Figure 20

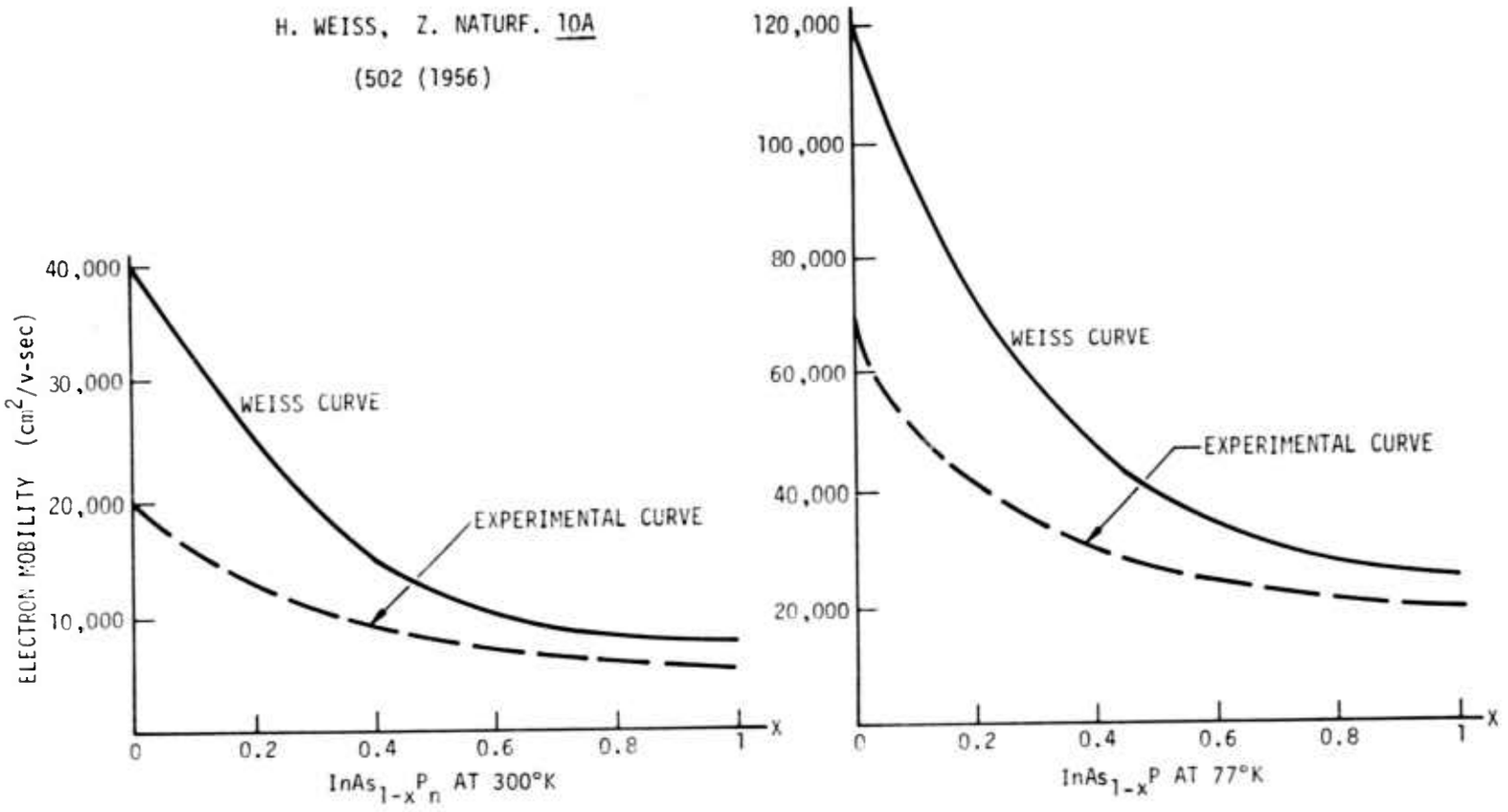
H. WEISS, Z. NATURF. 10A
(502 (1956)
ELECTRON MOBILITY (cm²/v-sec)
40,000
30,000
20,000
10,000
WEISS CURVE
EXPERIMENTAL CURVE
0
0.2
0.4
0.6
0.8
1
X
InAs1-xPn AT 300°K
120,000
100,000
80,000
60,000
40,000
20,000
WEISS CURVE
EXPERIMENTAL CURVE
InAs1-xP AT 77°K

Figure 21

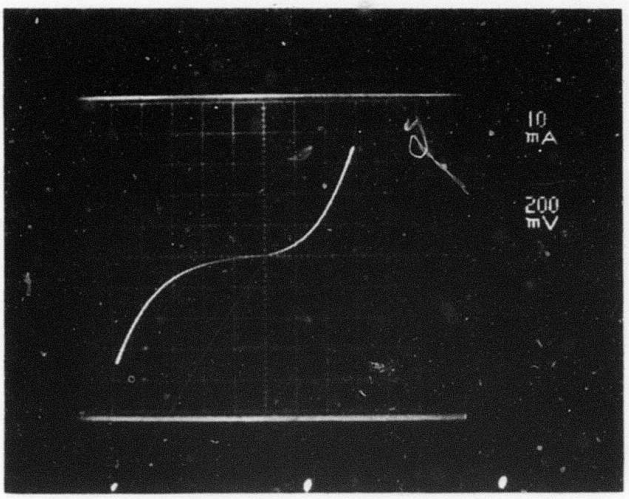

Figure 22a

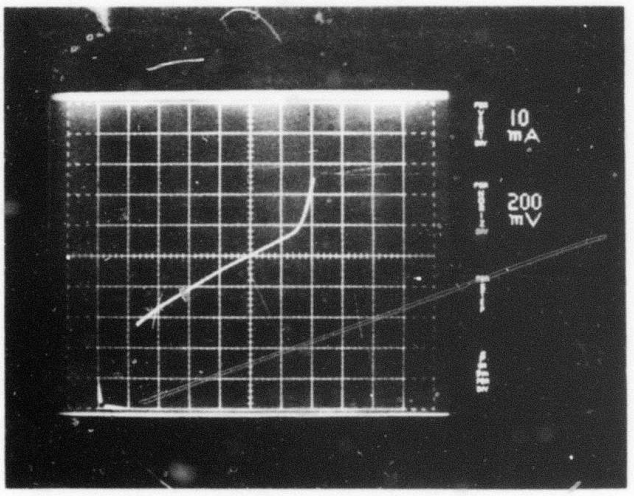

Figure 22b

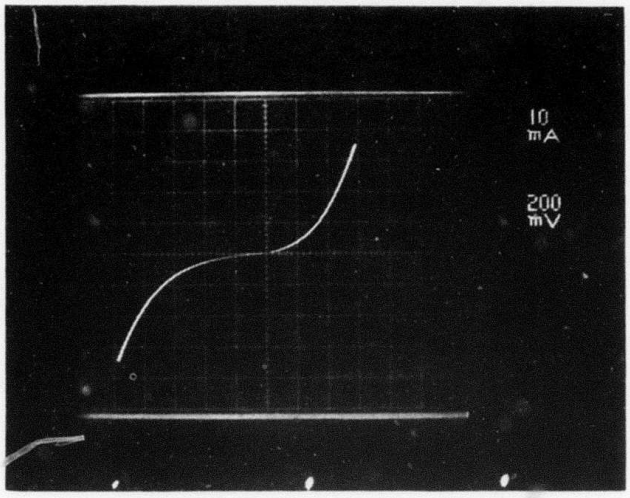

Figure 22a

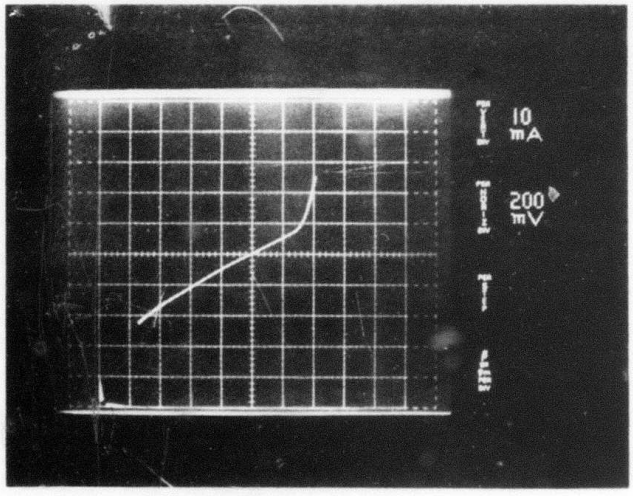

Figure 22b

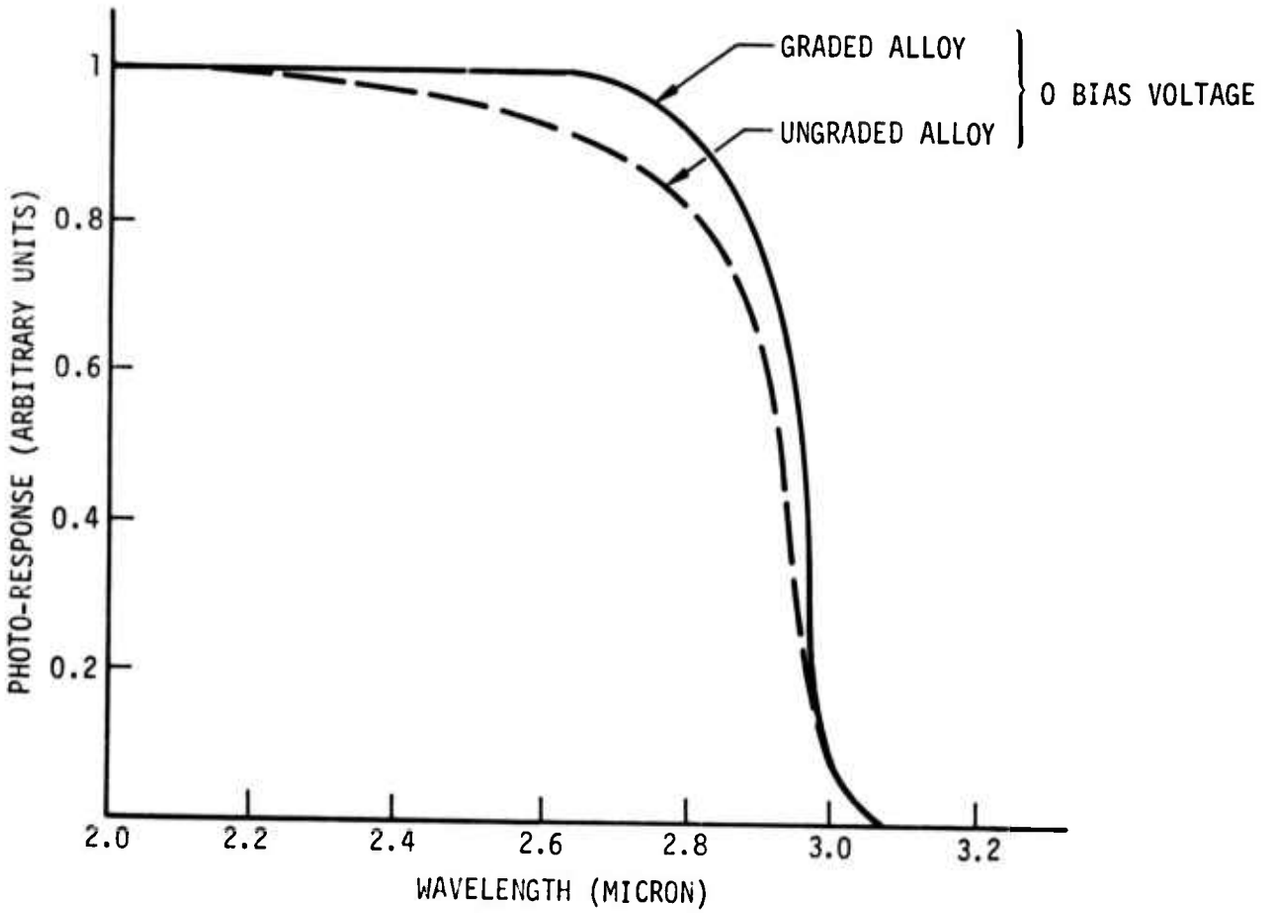
GRADED ALLOY
UNGRADED ALLOY
0 BIAS VOLTAGE
PHOTO-RESPONSE (ARBITRARY UNITS)
1
0.8
0.6
0.4
0.2
2.0
2.2
2.4
2.6
2.8
3.0
3.2
WAVELENGTH (MICRON)

Figure 23